PRESSURE, GAS RATIO AND OPERATION VOLTAGE OPTIMIZATION OF A HELIUM-NEON LASER

A THESIS SUBMITTED TO
THE GRADUATE SCHOOL OF NATURAL AND APPLIED SCIENCES
OF
MIDDLE EAST TECHNICAL UNIVERSITY

BY

HULUSİ BİROL BİLGİLİ

IN PARTIAL FULFILLMENT OF THE REQUIREMENTS
FOR
THE DEGREE OF MASTER OF SCIENCE
IN
PHYSICS

JANUARY 2005

Approval of the Graduate School of Natural and Applied Sciences

Prof. Dr. Canan Özgen
Director

I certify that this thesis satisfies all the requirements as a thesis for the degree of Master of Science.

Prof. Dr. Sinan Bilikmen
Head of Department

This is to certify that we have read this thesis and that in our opinion it is fully adequate, in scope and quality, as a thesis for the degree of Master of Science.

Assoc. Prof. Dr. Akif Esendemir
Supervisor

Prof. Dr.Raşit Turan	(METU, PHYS)	
Assoc. Prof. Dr. Akif Esendemir	(METU, PHYS)	
Assoc. Prof. Dr. Mehmet Parlak	(METU, PHYS)	
Dr. Yavuz Aka	(ROKETSAN A.Ş.)	
Dr. Ali Alaçakır	(Türkiye Atom Enerjisi Kurumu)	

I hereby declare that all information in this document has been obtained and presented in accordance with academic rules and ethical conduct. I also declare that, as required by these rules and conduct, I have fully cited and referenced all material and results that are not original to this work.

Name, Last name : Hulusi Birol BİLGİLİ

Signature :

ABSTRACT

PRESSURE, GAS RATIO AND OPERATION VOLTAGE OPTIMIZATION OF A HELIUM-NEON LASER

BİLGİLİ, Hulusi Birol
M.S., Department of Physics
Supervisor : Assoc. Prof. Dr. Akif Esendemir

January 2005, 50 pages

Aim of this thesis is to investigate the optimum working parameters of a helium-neon laser. Partial pressure ratios, total pressures of the gases and voltage-current characteristics were studied. The analysis of the results includes the minor factors (impurity, volume, etc.) and their effects to main parameters (laser power, voltage, current). Tables, which were formed by measured optical parameters as wavelength and power, converted to graphs and from these graphs optimal working conditions for the laser are obtained.

Keywords: HeNe Laser, Pressure, Gas Analysis, Getter

ÖZ

HELYUM-NEON LAZERDE; BASINÇ, GAZ ORANI VE ÇALIŞMA VOLTAJI OPTİMİZASYONU

BİLGİLİ, Hulusi Birol
Yüksek Lisans, Fizik Bölümü
Tez Yöneticisi : Doç. Dr. Akif Esendemir

Ocak 2004, 50 sayfa

Bu çalışmada helyum-neon lazerinin en iyi kazancı sağlayabilmesi için gerekli şartlar incelenmiştir. Yapılan deneylerde; gazların kısmi basınç oranı, toplam basınç değeri, voltaj-akım karakteristikleri incelenmiştir. Ortaya çıkan sonuçların analizi yapılmış olup çevresel faktörlerin (kirlilik, hacim,vs.) yukarıdaki parametrelerle ilişkisi incelenmiştir. Lazerde ölçülen dalga boyu, çıkış gücü gibi optik parametrelerin değerleri tablolar halinde verilmiş ve lazerin en iyi verimle çalışabilmesi için grafiklerde çalışma eğrileri oluşturulmuştur.

Anahtar Kelimeler: HeNe Lazer, Basınç, Gaz Analizi, Getter

In memory of my father…

ACKNOWLEDGMENTS

I would like to express my deepest gratitude to my supervisor Assoc. Prof. Dr. Akif Esendemir for his guidance, support, and criticism throughout the research.

I would like to express my sincere thanks to Dr.Ali Alaçakır for his support and advice in the laboratory.

I would like to thank Mr. Kazım Küçükturhan for his encouragement and support for my academic works.

I am very grateful to Mr. Salur Kurucu who supplied the laser tube for the experiments.

The technical assistance and kind help of Ms. Şafak Özcan, during the experiment, is gratefully acknowledged.

I would like to thank the members of Laser and Optoelectronics Laboratory for the time we shared and for their positive attitude towards me.

At last, but not the least, my mother, Türkan Bilgili deserves my deepest and genuine acknowledgements for all she does.

Thank you indeed.

TABLE OF CONTENTS

PLAGIARISM iii
ABSTRACT iv
ÖZ v
ACKNOWLEDGMENTS vii
TABLE OF CONTENTS viii
LIST OF TABLES x
LIST OF FIGURES xi
CHAPTER
1. INTRODUCTION 1
1.1. General Information 1
1.2. Objective of the Study 2
2. THEORY OF HELIUM-NEON LASER 3
2.1. HeNe Energy-Level Diagram 3
3. EXPERIMENTAL SYSTEM 16
3.1. Overview 16
3.2. Laser Tube 17
3.2.1. Getter 18
3.3. Vacuum System 19
3.3.1. Vacuum Pumps: 21
3.3.2. Vacuum Gauges: 22
3.4. Gas Analysis System 25
3.4.1. Basics of Residual Gas Analyzers 25
3.4.2. A Brief Note on Mass Units in Mass Spectrometry 26
3.4.3. Principles of RGA 27
3.5. Voltage Source 28
3.6. Optical Setup 28
3.7. Procedure 29

4. RESULTS AND DISCUSSION 33
4.1. Spectrum Measurements 33
4.2. Pressure-Ratio Measurements 35
4.3. Voltage-Current Measurements 38
5. SUMMARY AND CONCLUSION 41
5.1. Spectrum 41
5.2. Total Pressure and Gas Ratio 45
5.3. Voltage and Current 46
REFERENCES 48
APPENDIX 50

LIST OF TABLES

TABLES

Table 1.1: Most common gas laser types 1

Table 1.2: He/Ne gas ratio values in several publications 2

Table 2.1: Transitions and Laser lines 7

Table 3.1: Calibration factors for different gas types. 24

Table 3.2: Corrected pressure values for gas mixture preparation 31

Table 3.3: Atomic mass values for different residual materials. 32

Table 4.1: Power output of HeNe laser using the designated pressure values. 36

Table 4.2: Current and pressure values of gas discharge 39

Table A.1: Spectrum of HeNe Laser 50

LIST OF FIGURES

FIGURES

Figure 2.1: Energy-level diagram for helium and neon 3

Figure 2.2: The most important laser transitions in the neon system 5

Figure 2.3: Modern HeNe laser with glass-to-metal soldering of the anode, cathode and laser mirror 8

Figure 2.4 : Probability Distribution for the velocity v of the neon atoms in between v and v + dv interval 9

Figure 2.5 : Inhomogeneous line profile, speed intervals dv 10

Figure 2.6 : Decay of the population of state 2 into a state 1 with lower energy 11

Figure 2.7 : Natural linewidth (FWHM) caused by spontaneous emission 12

Figure 2.8 : Natural broadened line profiles (homogeneous) for groups of speed within the inhomogeneous Doppler broadened gain profile 12

Figure 2.9 : Population inversion and transition between sub-ensembles with same velocity v 13

Figure 2.10 : Standing longitudinal waves in an optical resonator. A with n nodes and B with n+3 nodes 14

Figure 2.11 : Inhomogeneous gain profile (Gaussian profile)interacting with an optical resonator 15

Figure 3.1: Block diagram of the experimental construction 16

Figure 3.2: Photo taken while the lasing action 17

Figure 3.3: Tube end, before and after soldering. 17

Figure 3.4: Getter of the laser tube 19

Figure 3.5: Vacuum system 20

Figure 3.6: CF flange connections. 20

Figure 3.7: Mechanical and turbomolecular pumps that are used in the experiment. 21

Figure 3.8: Inficon Pirani Gauge 22

Figure 3.9: Gas type dependence for Pirani sensor 23

Figure 3.10: Inficon Bayard-Alpert Pirani Combination Gauge 24

Figure 3.11: A view from the RGA software 25

Figure 3.12: Stanford RGA 27

Figure 3.13: HV power supply 28

Figure 3.14: Optical power measurement setup 28

Figure 3.15: Schematic diagram of the vacuum system 30

Figure 3.16: Background impurities in the vacuum system. 32

Figure 4.1: Spectrum of HeNe laser at its peak power. 33

Figure 4.2 : Spectrum of the HeNe laser 34

Figure 4.3: Spline smoothed output power for different He/Ne pressure. 37

Figure 4.4: Voltage-current behavior of the gas discharge 39

Figure 4.5: Current characteristics of the HeNe gas discharge 40

Figure 5.1: Residual Gas Measurement of the tube and the spectrum measurement of the laser (RG1) 42

Figure 5.2: Residual Gas Measurement of the tube and the spectrum measurement of the laser (RG2) 43

Figure 5.3: Residual Gas Measurement of the tube and the spectrum measurement of the laser (RG3) 44

Figure 5.4: Spectrum graph of the laser, containing different amount of residual gases 45

Figure 5.5: Behavior of output power with different gas pressures and ratios. 46

Figure 5.5: Operating current characteristics with different pressure values. 47

CHAPTER 1

INTRODUCTION

1.1. General Information

Laser is an acronym formed from Light Amplification by Stimulated Emission of Radiation. According to lasing media properties laser can be categorized as gas, solid state and dye lasers. The helium-neon laser is the most common gas laser, which was invented in 1961 by Ali Javan [1]. Javan's first He-Ne laser lased at a wavelength of 1.5μm that was invisible to the human eye. Only one year later 632 nm lasing was obtained from the HeNe gas laser by White and Ridgen [15]. This is the one of the gas lasers (Table 1.1) which is now commonly known as the red line. It is now clear that HeNe lasers will have to increasingly compete with laser diodes in the future. But HeNe lasers are still unequalled as far as beam geometry and the purity of the modes are concerned. Laser diodes will have to be improved to a great extent before they pose a serious threat to He-Ne lasers.

Table 1.1: Most common gas laser types

ATOM	*MOLECULE*	*ION*	*METAL VAPOR*
• He-Ne • He-Cd	• CO_2 • N_2 • Chemical • Excimer	Ar+ Kr+	Cu Vapor Ag Vapor

1.2. Objective of the Study

helium-neon laser is a key factor for metrology applications that needs to have stable output power and good beam geometry. For a stable HeNe laser the main parameters are mixing ratio, pressure and operating voltage. The operating voltage and the pressure are related to each other but the gas ratios are mainly dependent on the transition mechanism and population inversion of the laser. When the current publications are examined it is seen that the He/Ne ratio is not a constant value (Table 1.2).

Table 1.2: He/Ne gas ratio values in different laser types

Books & Papers	
He/Ne Ratio	***Author***
9	Bloom
5	Hawkes
5 to 12	Hecht
5	Svelto
10	Silfvast
3.5	Chartier
7	Hânsc
11	Lindström

Commercial Lasers	
He/Ne Ratio	***Company***
7,5	LEOT
10	J & K
5 to 12	Industrial Fiber Optics
10	LEOS

This thesis includes the experiments carried out to obtain the optimum gas ratio and pressure conditions for a helium-neon laser. The voltage and current characteristics are also studied to obtain the optimum voltage-current parameters. Effects of residual gas formed a secondary parameter to be investigated.

CHAPTER 2

THEORY OF HELIUM-NEON LASER

2.1. HeNe Energy-Level Diagram

The fascination for inert gases and their clear atomistic structure formed the basis for many spectroscopic investigations. The knowledge obtained through spectroscopic data was extremely helpful in deciding to choose helium and neon for the first lasers, using Schawlow Towne's discovery of lasing conditions in 1958 to estimate whether an inversion was feasible in laser operation. The lifetime of the s- and p-states were well known. Those of the s-states were longer than those of the p-states by a factor of about 10. The inversion condition was therefore fulfilled.

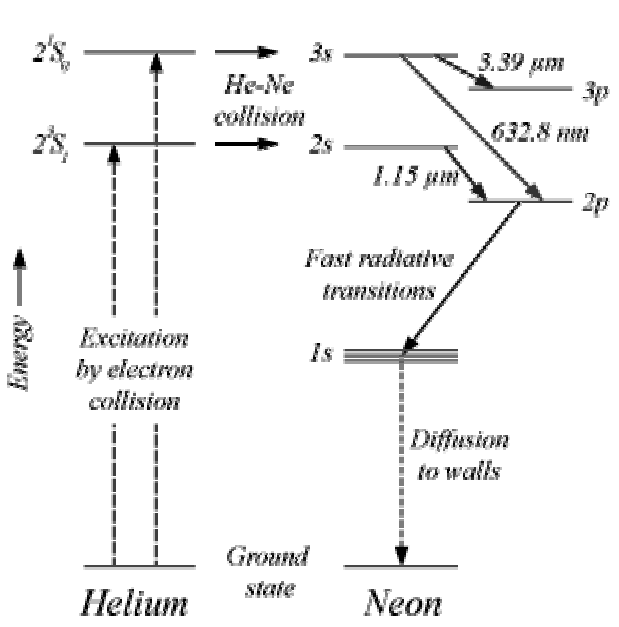

Figure 2.1: Energy-level diagram for helium and neon

Fig. 2.1 shows the reduced energy-level diagram for helium and neon. Only those levels important in the discussion of the excitation and laser processes at a wavelength of 632 nm are indicated. The left side of the representation shows the lower levels of the helium atoms.

A characteristic of helium is that its first states to be excited, 2^1S_1 and 2^1S_0 are metastable, i.e. optical transitions to the ground state 1^1S_0 are not allowed, because this would violate the selection rules for optical transitions. As a result of gas discharge, these states are populated by electron collisions. A collision is called a collision of the second type if one of the colliding bodies transfers energy to the other so that a transition from the previous energy state to the next higher or lower takes place. Apart from the electron collision of the second type there is also the atomic collision of the second type. In the latter, an excited helium atom reaches the initial state because its energy has been used in the excitation of a Ne atom. Both these processes form the basis for the production of a population inversion in the Ne system.

It is seen that in Fig. 2.1, the 2^1S_0 is slightly below the 3s level of the neon. However, the additional thermal energy kT is sufficient to overcome this gap. As already mentioned, the lifetime of the s-states of the neon are approximately 10 times longer as those of the p-states. An immediate population inversion between the 3s and the 2p levels will therefore be generated. The 2s level is emptied due to spontaneous emission into the 1s level. After this the neon atoms reaching their ground state again, primarily through collisions with the tube wall (capillary), since an optical transition is not allowed. This calming down process is the bottleneck in the laser cycle. It is therefore advisable to choose a capillary diameter that is as small as possible. However, the laser will then suffer more losses. Modern He-Ne lasers work at an optimum of these contradictory conditions. This is the main reason for the comparatively low output of He-Ne lasers.

The laser cycle of the commonly known red line at 632 nm is discussed up to this point. However the neon has several other transitions, used to produce about 200 laser lines in the laboratories. The following explanation describes the energy-level diagram for further visible lines.

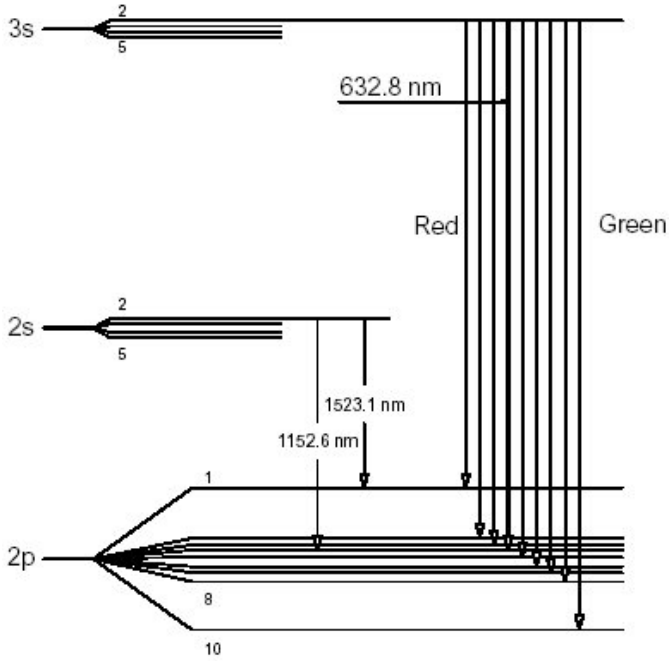

Figure 2.2: The most important laser transitions in the neon system

The 3s state is populated by helium atoms of the 2^1S_0, state as a result of an atomic collision. The 3s state consists of 4 sub-states out of which it is primarily the $3s_2$ state which has been populated through the collision process. The population density of the other 3s sub-states is approximately 400 times less than that of the $3s_2$ state [14]. The 2s state is populated by the helium atoms of the 2^3S_1, as a result of an atomic collision.

The four sub-states of the 2s group are all populated in a similar way. Visible (VIS) optical transitions and laser processes are taking place between the $3s_2 \rightarrow 2pi$ and infrared (IR) between the $2si \rightarrow 2pi$ energy levels. The following table shows the most important laser transitions. The Einstein coefficients A_{ik} are given for the visible lines and amplification is indicated as a percentage per meter.

Further laser transitions are known, which start at the 3s2 level and terminating at the 3p level of the neon. However, these laser transitions lie even further within the infrared spectral range and cannot be detected with the silicon detector used in the experiments so they are not particularly suitable for experiments. Since the cross-section of the stimulated emission is increasing with λ^3 as well, the amplification of these lines is therefore very strong. This applies to the 3.39 µm line in particular, which, due to a sufficiently long capillary, shows laser activity (so called super fluorescence) even without an optical resonator [9].

Table 2.1: Transitions and Laser lines [2]

Transition	**Wavelength [nm]**	**A_{ik} [10^8 s^{-1}]**	**Gain [%/m]**
3s2→2p1	730.5	0,00255	1,2
3s2→2p2	640.1	0,0139	4,3
3s2→2p3	635.2	0,00345	1,0
3s2→2p4	632.8	0,0339	10,0
3s2→2p5	629.4	0,00639	1,9
3s2→2p6	611.8	0,00226	1,7
3s2→2p7	604.6	0,00200	0,6
3s2→2p8	593.9	0,00255	0,5
3s2→2p9	N/A	-	-
3s2→2p10	543.3	0,00283	0,52
2s2→2p1	1523.1		
2s2→2p2	1177.0		
2s2→2p3	1160.5		
2s2→2p4	1152.6		
2s2→2p5	1141.2		
2s2→2p6	1084.7		
2s2→2p7	1062.3		
2s2→2p8	1029.8		
2s2→2p9	N/A	-	-
2s2→2p10	886.5		
2s3→2p2	1198.8		
2s3→2p5	1161.7		
2s3→2p7	1080.1		

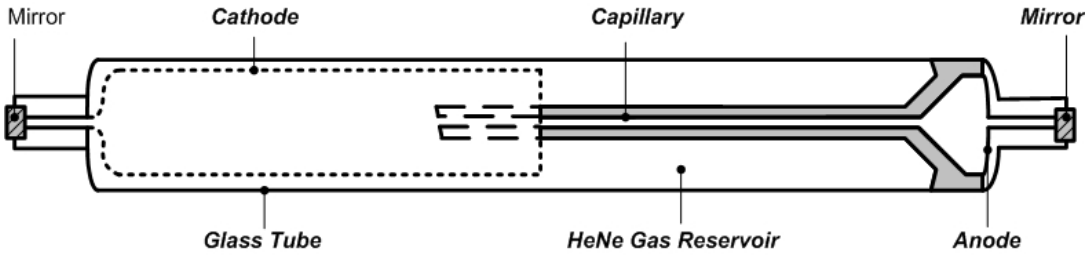

Figure 2.3: Modern HeNe laser with glass-to-metal soldering of the anode, cathode and laser mirror

Fig. 2.3 shows a modern laser tube made with highly perfected manufacturing techniques and optimized to suit the physical aspects of the laser. This applies to the resonator in particular, which is designed for a best possible output in the fundamental mode with a purely Gaussian beam and spectral purity in single mode operation (e.g. for interferometric length measurement). The fulfillment of this demand depends, among other aspects, on the optimal adaptation of the resonator to the amplification profile of the neon. The behavior of neon during amplification will therefore be discussed first.

The neon atoms move more or less freely in the laser tube but at different speeds. The number N of neon atoms with the mass m, within a speed interval of v to v+dv is described according to the Maxwell-Boltzmann distribution (Fig. 2.4).

$$\frac{n(v)}{N} = \frac{4}{\sqrt{\pi}} \cdot \frac{v^2}{\sqrt[3]{(2kT/m)^2}} \cdot e^{-\frac{mv^2}{k \cdot T}} dv \qquad (2.1)$$

T is the absolute temperature and k Boltzman´s constant. The above equation is applicable for all directions in space. However, our only interest is the distribution of speed in the direction of the capillary. Using $v^2 = v_x^2 + v_y^2 + v_z^2$ we obtain for the direction x:

$$\frac{n(v_x)}{N} = \sqrt{(2kT/m)} \cdot e^{-\frac{m \cdot v^2}{k \cdot T}} dv_x \qquad (2.2)$$

A resting observer will now see the absorption or emission frequency shifted, due to Doppler's effect, and the value of the shift will be:

$$\nu = \frac{\nu_0}{1 \pm v/c} \quad \text{assuming } v << c \tag{2.3}$$

ν_0 is the absorption or emission frequency of the resting neon atom and c the speed of light. If the Doppler equation (Eq. 2.3) is used to substitute the velocity v in the Maxwell-Boltzmann´s velocity distribution (Eq. 2.2) the line broadening produced by the movement of neon atoms can be found [13]. Since the intensity is proportional to the number of absorbing or emitting neon atoms, the intensity distribution will be:

$$I(v) = I(v_0) \cdot e^{-\left(c \cdot \frac{v - v_0}{v_0 \cdot v_w}\right)^2} \tag{2.4}$$

v_w is the most likely speed according to:

$$v_w = \sqrt{\frac{2kT}{m}} \tag{2.5}$$

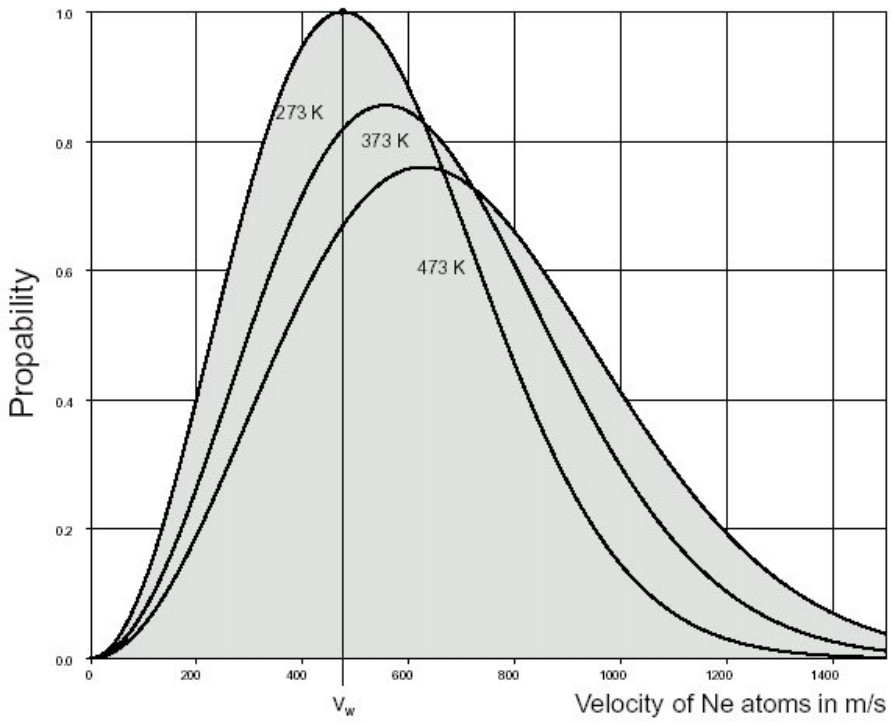

Figure 2.4 : Probability Distribution for the velocity v of the neon atoms in between v and v + dv interval.

The full width at half maximum is calculated by setting

$$I(\nu)=1/2\ I(\nu_0) \tag{2.6}$$

and the result is:

$$\Delta\nu_{Doppler} = \sqrt{\ln 2}\cdot\frac{v_w}{c}\cdot\nu_0 \tag{2.7}$$

It can be concluded from Eq. 2.7 that the line broadening caused by Doppler's effect is larger in the case of:

higher resonance frequencies ν_0

or smaller wavelengths ($\nu_0=c/\lambda_0$, UV-lines)

higher most likely velocity v_w

that means higher temperature T

and smaller in the case of:

a larger particle mass.

The line profile also corresponds to a Gaussian distribution curve (Eq. 2.4). Fig. 2.5 shows this kind of profile. The histogram only approaches the distribution curve when the speed interval dv is small enough.

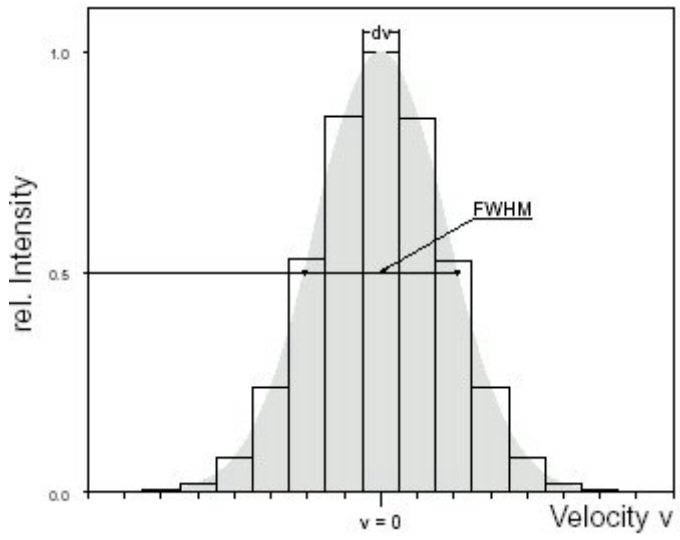

Figure 2.5 : Inhomogeneous line profile, speed intervals dv

On closer observation it can be seen that a line broadened by the Doppler effect actually does not have a pure Gaussian distribution curve. To understand this, an ensemble of Ne atoms picked out whose speed components have the value v in the direction of observation. It is expected that all these atoms emit light with the same frequency ν or wavelength λ. But an additional effect should be considered that is responsible for the natural linewidth of a transition. It is known that each energy level poses a so-called lifetime. The population n_2 of a state 2 decays into a state 1 with lower energy with a time constant τ_s following the equation:

$$n_2(t) = n_2(t=0) \cdot e^{-A_{21} \cdot t} \quad \text{with } \tau_s = 1 / A_{21} \tag{2.8}$$

A_{21} is the Einstein coefficient for the spontaneous emission. The emission which takes place is termed as spontaneous emission.

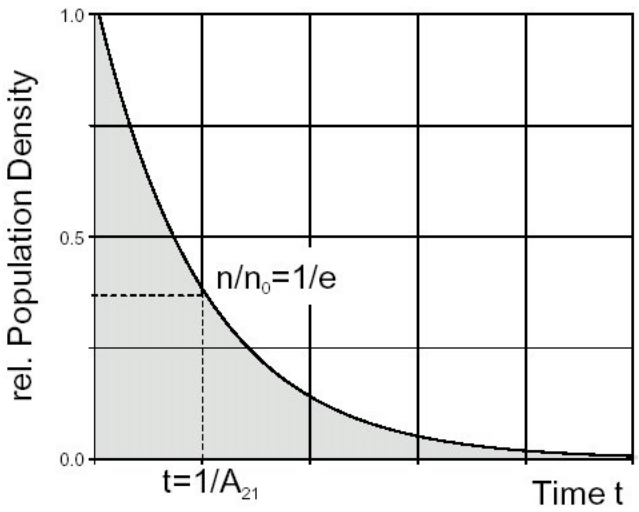

Figure 2.6 : Decay of the population of state 2 into a state 1 with lower energy

This shows that the ensemble of Ne atoms does not emit light at a single frequency. It emits a frequency spectra represented by a Lorentz profile (Fig. 2.7).

$$\delta(\nu) = \frac{1}{4\pi \cdot (\nu - \nu_{21})^2 + (1/2 \cdot \tau_s)^2}, \nu_0 \equiv \nu_{21} \tag{2.9}$$

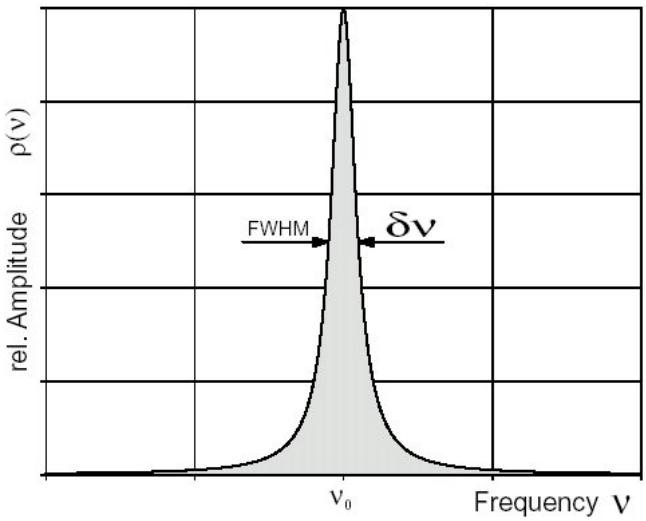

Figure 2.7 : Natural linewidth (FWHM) caused by spontaneous emission

The exact profile formation can be determined from the convolution of the Gaussian profile with the individual Lorentz profiles. The result obtained in this manner is called as the Voigt profile. Since one group of particles in an ensemble can be assigned to a given speed v, these groups have characteristics that differentiate them. Every group has its own frequency of resonance. Which group a photon interacts with depends on the energy (frequency) of the photon. This does not affect the other groups which are not resonant on this interaction. Therefore such kind of a gain profile is termed inhomogeneous.

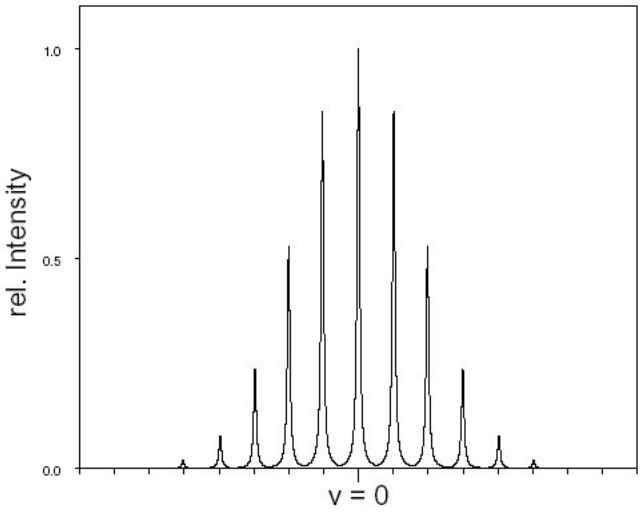

Figure 2.8 : Natural broadened line profiles (homogeneous) for groups of speed v within the inhomogeneous Doppler broadened gain profile

The gain occurs in a medium when it shows inversion. This means that the population density of the upper level n_2 (3s in the Ne-system) is larger than the population density of the lower state n (2p). In Fig. 2.9 the population profiles are rotated by 90° to draw them in the well known energy level diagram.

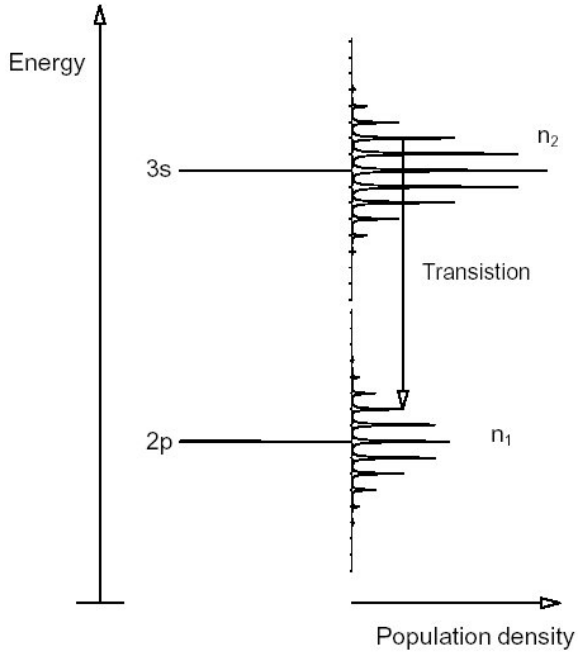

Figure 2.9 : Population inversion and transition between sub-ensembles with same velocity v

The situation of Fig. 2.9 shows a population inversion $n_2 > n_1$. Besides some specific other constants the gain is proportional to the difference $n_2 - n_1$. If the inverted ensemble of Ne atoms is considered to place into an optical cavity, which is formed by two mirrors having the distance of L. Due to the spontaneous emission photons are generated which will be amplified by the inverted medium and reflected back from the mirrors undergoing a large number of passes through the amplifying medium. If the gain compensates for the losses, a standing laser wave will be built up inside the optical resonator. Such a standing wave is also termed as oscillating mode of the resonator also eigenmode or simply mode. Every mode must fulfill the following condition:

$$L = n \cdot \frac{\lambda}{2} \quad \text{or} \quad L = n \cdot \frac{c}{2\nu} \tag{2.10}$$

L represents the length of the resonator, λ the wavelength, c the speed of light, ν the frequency of the generated light and n is an integer number. Thus every mode has its frequency of

$$\nu(n) = n \cdot \frac{c}{2L} \tag{2.11}$$

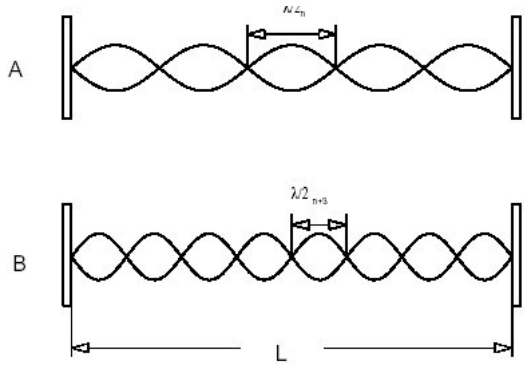

Figure 2.10 : Standing longitudinal waves in an optical resonator.
A with n nodes and B with n+3 nodes

For a HeNe laser with a resonator length of 30 cm at an emission wavelength λ of 632.8 nm will have the following value for n:

$$n = \frac{v}{c} \cdot 2 \cdot L = 2 \cdot \frac{L}{\lambda} = 2 \cdot \frac{0{,}3}{632{,}8 \cdot 10^{-8}} = 949{,}167 \tag{2.12}$$

The difference in frequency of two neighbored modes is:

$$\Delta v = v(n+1) - v(n) = (n+1) \cdot \frac{c}{2L} - n \cdot \frac{c}{2L} = \frac{c}{2L} \tag{2.13}$$

In the above example the distance between modes would be

$$\Delta v = \frac{3 \cdot 10^8}{2 \cdot 0{,}3} = 5 \cdot 10^8 \,\text{Hz} = 500\text{Mhz} \tag{2.14}$$

If the active laser material is now brought into the resonator standing waves will be formed due to the continuous emission of the active material in the resonator and energy will be extracted from the material. However, the resonator can only extract energy for which it is resonant. Strictly speaking, a resonator has an indefinite amount of modes, whereas the active material only emits in an area of frequency determined by the emission line width. Fig. 2.11 shows the situation in the case of material that is in homogeneously broadened.

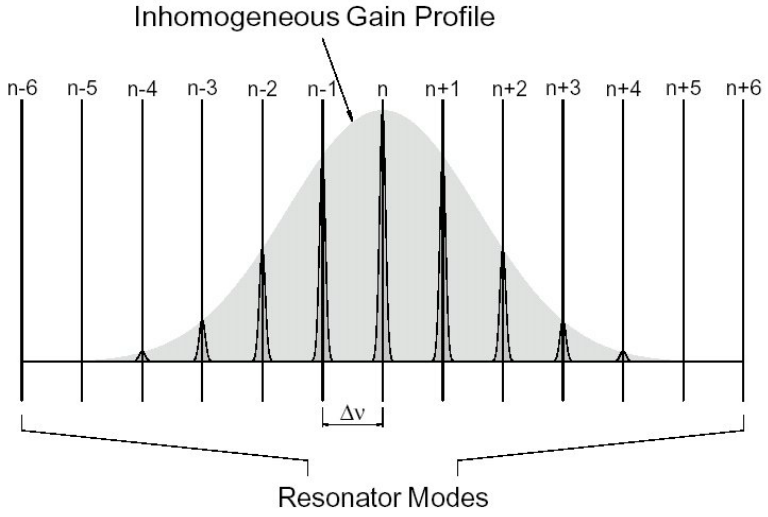

Figure 2.11 : Inhomogeneous gain profile (Gaussian profile) interacting with an optical resonator

If the laser is operating in a stationary state, it can be seen that it is emitting several longitudinal modes. These are exactly the same modes that will be found in the emission profile. Since the modes are fed by an inhomogeneous emission profile they can also exist independently. The HeNe laser is a classic example of this.

CHAPTER 3

EXPERIMENTAL SYSTEM

3.1. Overview

The constructed HeNe Laser system can be classified as follows (Fig 3.1);

- Laser tube
- Vacuum system
- Gas analysis system
- Voltage Source
- Optical Powermeter and Spectrometer

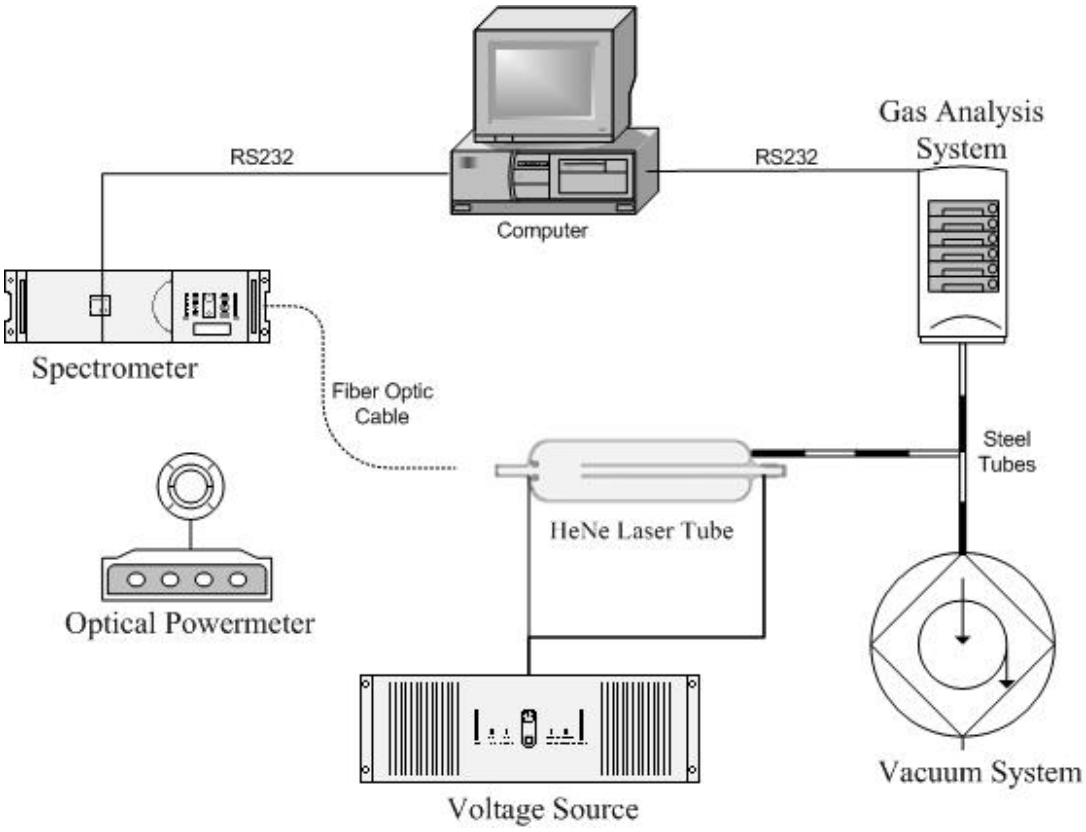

Figure 3.1: Block diagram of the experimental construction

3.2. Laser Tube

In the experiment Carl Zeiss Jena (LGR 7627 M) HeNe tube (Fig.3.2) is used.

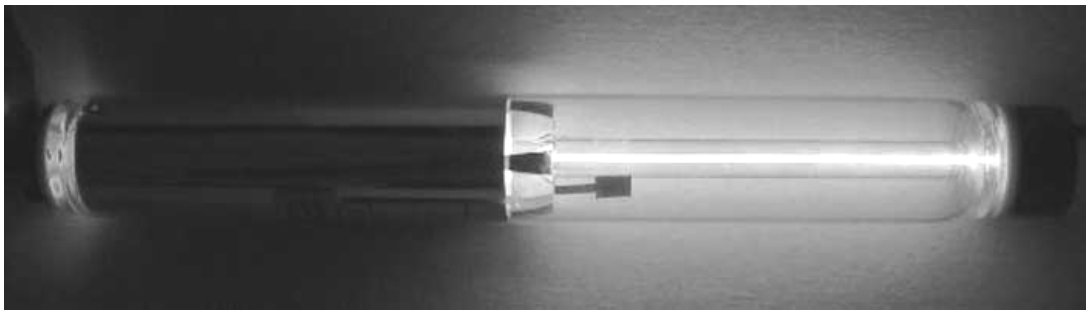

Figure 3.2: Photo taken while the lasing action

In most of the HeNe lasers the gas filling is done through a metal tube and than the pipe is closed by squeezing the end. To use this laser, the metallic gas insertion tube near the anode is bored in the machine workshop. Then a copper tube, with ¼" outer diameter, is silver soldered to have a vacuum tight connection (Fig 3.3). The tube is connected to the vacuum system by using Swagelok© tube connections, valve and NPT/KF adaptors. The rest of the system is designed to have KF flanges with Viton© o-rings.

Figure 3.3: Tube end, before and after soldering.

The output coupler and high reflector mirrors are “hard sealed” to tube for long life and alignment-free operation. The mirrors are fused to their respective mounts by a special glass frit (glass solder). These seals do not leak - at least not on any time scale that matters. Thus the shelf life of hard sealed tubes is essentially infinite.
The frit is basically powdered low melting point glass mixed with a liquid to permit it to be spread like painted on. The frit can be fired at a low enough temperature that the mirror mount or glass mirror itself is not damaged so there is virtually no distortion introduced by the process, and manufacturing is greatly simplified compared to using normal (high temperature) glass or ceramic joints. Some tubes use frit seals at other locations in addition to the mirrors (like the end-caps) rather than glass-to-metal seals. The same process is used for permanently sealed other gas laser tubes like those in internal mirror argon ion lasers as well as some xenon flashlamps and similar devices.

3.2.1. Getter

In lasers ultra pure gases need to be used to decrease the line broadening and increase the output power. In most of the cases, because of the vacuum system components, some impurities can occur [6]. In the commercial laser tubes getters are used to purify the gas in the tube.

Bulk getters are sheets or wires of gas-absorbing metals, which are usually heated for this purpose by mounting them on hot electrodes of the tube. In some cases the heating is accomplished by a separate heat source. There are mainly two ways to activate the getters; one is DC voltage application. Especially in the old cathode tubes the getters are activated by applying voltage to the ends of the cables which are outside the tube. But the most common technique is to use RF induction heating with a coil close to the getter.

Getter gas purifiers use two processes to remove impurities, adsorption and bulk diffusion. Impurities adsorb onto the surface of the getter material in the first step. The heated getter then allows the impurities to diffuse into the bulk of the getter material, binding it to the substrate. The reaction is irreversible, so the impurities cannot be released back into the gas stream. Getter purifiers remove O_2, H_2O, CO, CO_2 and N_2 [10]. The getter is consumed during use, but the bulk diffusion provides very high capacities leading to long lifetimes.

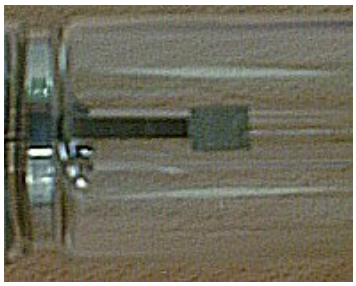

Figure 3.4: Getter of the laser tube

During the processes the getter (Fig. 3.4) is not used because of frequent need of gas change for the experiments. Since so many gas pressures and ratios are tested (≈50 different models), the nature of the getter make it impossible to use it one after the other. The effects of residual chemicals to the spectra are discussed in the results chapter.

3.3. Vacuum System

Vacuum system (Fig 3.5) consists of several parts like mechanical pump, turbo molecular pump, gauges and controllers, temperature sensors, block and needle valves. All these components are chosen to obtain and test the high vacuum conditions.

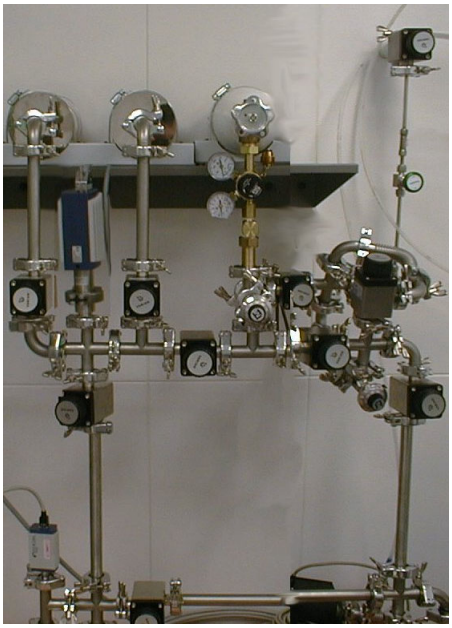

Figure 3.5: Vacuum system

The system is designed to have copper gaskets with CF flange system but later during the system construction it is seen that to use them everywhere is not practical because they reduce the flexibility to play with the experimental setup. So only the parts above the turbomolecular pump are connected with CF flanges (Fig. 3.6). The rest of the system is constructed with KF flange system that makes it possible to obtain the high vacuum.

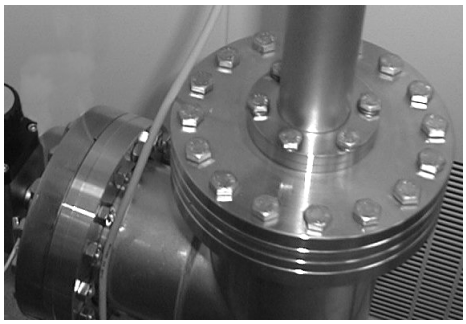

Figure 3.6: CF flange connections.

3.3.1. Vacuum Pumps:

In order to obtain high vacuum Varian Turbo 551 Navigator (Fig. 3.7) turbomolecular pump is used. Turbomolecular pumps use a rapidly spinning turbine rotor to push gas from the inlet of the pump. Most turbomolecular pumps employ multiple stages consisting of rotor/stator pairs mounted in series. Gas captured by the upper stages is pushed into the lower stages and successively compressed to the level of the fore-vacuum pressure.

A mechanical vacuum pump is needed to reduce the exhaust pressure and start a turbomolecular pump. So a Varian DS 402 pump (Fig. 3.7) is used to obtain required fore-vacuum pressure.

Figure 3.7: Mechanical and turbomolecular pumps that are used in the experiment.

Unfortunately, the compression ratio varies exponentially with the square root of the molecular weight of the gas. Thus, heavy molecules are pumped much more efficiently than light molecules. Most gases are heavy enough to be well pumped but it is difficult to pump efficiently helium gas.

Anti-suckback filters are used to reduce the contamination caused by motor oil

3.3.2. Vacuum Gauges:

Two types of gauges are used in the vacuum system; for the low vacuum Pirani Standard Gauge (Fig 3.8) is used that have been designed for vacuum measurement of gases in the pressure range of 5×10^{-4} to 1000mbar. But it is effective on the scales below 10^{-3} mbar.

Figure 3.8: Inficon Pirani Gauge

In conventional Pirani gauges the filament used as measurement element is one arm of a self-adjusting bridge circuit. The filament temperature in the range of 120 ^{o} C. Whenever a pressure change occurs a gain control amplifier automatically adjusts the bridge voltage to keep the filament temperature constant. This bridge excitation is the primary measurement used in determining the pressure. The ambient operating temperature also has an influence on the power necessary to keep the filament temperature constant. Ambient temperature changes appear as changes in pressure. To compensate, a temperature sensitive element is placed close to the sensor. The ambient temperature is registered and the measurement signal is compensated, accordingly.

This sensor consists of two filaments, which are kept constant at two separate operating temperatures (65^{o}-120 C). A change in pressure affects both filaments the same way. The power required to keep the filaments at the constant temperature is pressure dependent. By using the power difference between the two filaments one can easily eliminate changes in the temperature and thus isolate the changes in pressure. This satisfies the need for temperature compensation, but eliminates the delays associated with using a separate temperature sensor, resulting in a very fast response time [8].

As a result, to prepare a gas mixture it is seen that the most reliable gauge, for low vacuum, is a Pirani gauge. But an important point is that the indicated pressure value depends on the type of gas. To correct these values for helium and neon, the standard calibration curves (Fig 3.9) for Pirani sensor is used.

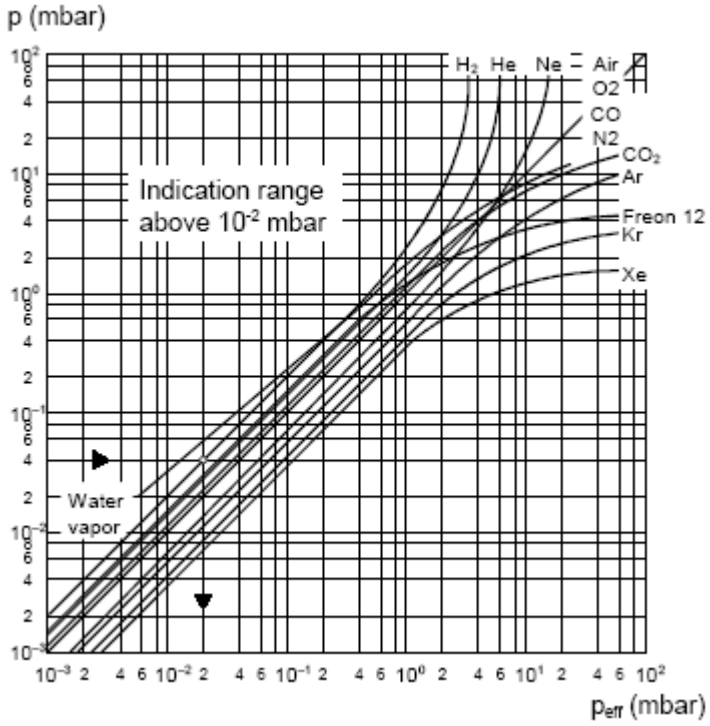

Figure 3.9: Gas type dependence for Pirani sensor [3]

For the pressure range below 1 mbar the calibration factor can be calculated as;

$$P_{eff.} = C \times P_{ind.} \qquad (3.1)$$

The calibration factors are given in Table 3.1.

Table 3.1: Calibration factors for different gas types. [3]

Gas Type	Calibration Factor
He	0.8
Ne	1.4
Air, O_2, N_2	1.0
CO_2	0.9
Water Vapor	0.5

For the high vacuum measurements Varian Bayard-Alpert Pirani Combination Gauge (Fig. 3.10) is used which provides the functions of two gauges in a single compact unit measuring from atmosphere to 3.8 x 10^{-10} Torr. The integrated Pirani protects the hot ion filament from burning out and reduces the contamination by automatically switching it off at high pressures.

Figure 3.10: Inficon Bayard-Alpert Pirani Combination Gauge

Conventional hot ion gauges used for high vacuum measurement can only be operated below atmospheric pressures typically in the range below 10^{-2} mbar. When operated at higher pressures the filament lifetime is dramatically reduced and may burn out almost immediately. Therefore, hot ion gauges must be switched on only at specified operating pressures. Usually, a fore vacuum gauge (Pirani) controls the switching on and off of the hot ion gauge. Such systems consist of two gauges with the necessary tubing, cabling and corresponding costly signal processing, which is done by PLC software or hardwiring.

Bayard-Alpert Pirani Combination Gauge consists of two sensing systems, a hot ion sensor and a Pirani sensor, which signals are combined in one single compact package. The Pirani sensor automatically controls the switching on and off of the hot ion sensor at a defined switching threshold [4]. The filament therefore is protected since the hot ion sensor is switched off instantaneously in case of an air inrush. This minimizes problems associated with operator error, extended signal processing time, and other system failures.

3.4. Gas Analysis System

3.4.1. Basics of Residual Gas Analyzers

Complete characterization of a vacuum environment requires the detection of all the component gases present (Fig. 3.11), as well as measurement of the total pressure. The instruments used for this purpose are called Residual Gas Analyzers or Partial Pressure Analyzers.

A Residual Gas Analyzer (RGA) is mass spectrometer of small physical dimensions that can be connected directly to a vacuum system and whose function is to analyze the gases inside the vacuum chamber.

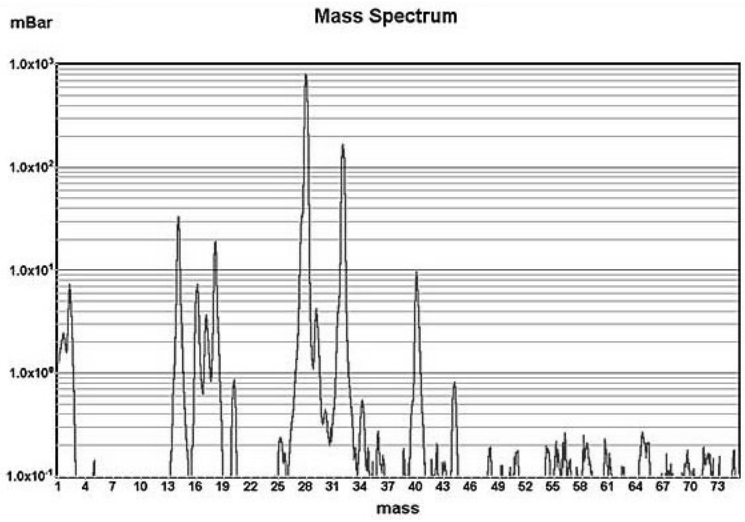

Figure 3.11: A view from the RGA software

The principle of operation is the same for all RGA instruments: A small fraction of the gas molecules are ionized (positive ions), and the resulting ions are separated, detected and measured according to their molecular masses.

RGA's are widely used to quickly identify the different molecules present in a residual gas environment and, when properly calibrated, can be used to determine the concentrations or absolute partial pressures of the components of a gas mixture.

3.4.2. A Brief Note on Mass Units in Mass Spectrometry

Since molecules are so small, it is convenient to define a special type of mass units to express the masses of individual ions. The atomic mass unit (amu), defined as 1/12 of the mass of a single carbon atom, isotope 12 (i.e. 12C), is the unit of molecular mass most commonly used in mass spectrometry (1 amu = 1.660 540 x 10^{-27} kg). To a very accurate approximation, the mass of a molecule in atomic mass units (amu) is equal to its mass number M, defined as the sum of the number of protons and neutrons in the molecule.

Mass spectrometers do not actually measure the molecular mass directly, but rather the mass-to-charge ratio of the ions. The mass-to-charge ratio, M/Q, is defined as the ratio of the mass number M of the ion to its charge Q, measured in units of the electron charge ē. For example: doubly charged ions of argon isotope 36 ($^{36}Ar^{2+}$) and singly charged ions of water, $^{1}H_2$ $^{16}O^{1+}$, have M/Q = 18, and cannot be differentiated from each other with most mass spectrometers.
For singly charged ions, the mass to charge ratio is numerically equal to the mass of the ion in atomic mass units (amu).

RGA users often use the term "mass of an ion" when they really mean the mass-to charge ratio. This convenient way of speaking is strictly valid for singly charged ions only.

3.4.3. Principles of RGA

The SRS RGA (Fig.3.12) is a mass spectrometer that analyzes residual gases by ionizing some of the gas molecules (positive ions), separating the resulting ions according to their respective masses and measuring the ion currents at each mass. Partial pressure measurements are determined with the help of previously calculated sensitivity (i.e. calibration) factors by reference to the abundance of the individual mass numbers attributed to each gas type.

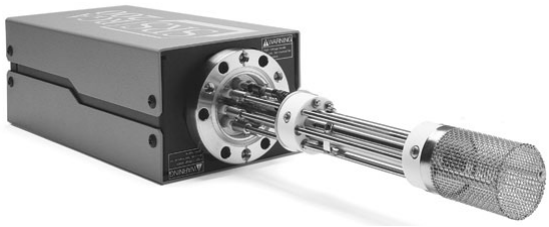

Figure 3.12: Stanford RGA

During analysis, positive ions are formed within the ionizer and directed towards the spectrometer's quadrupole mass-filter. The mass filter determines which ions reach the detector at any given time. It is operated by a combination of RF and DC voltages and the filtering action is based on the mass-to-charge dependency of the ion trajectories on the RF and DC fields. The magnitude and frequency of the RF determine the mass-to-charge ratio of the ions that can pass through the filter without striking the rods (i.e. with stable oscillations). The RF/DC ratio determines the filter selectivity. Ions that successfully pass through the filter are focused towards the detector and the resulting analog current is measured by the very sensitive electrometer [7].

3.5. Voltage Source

Gas lasers are ignited with high voltage DC power supplies. Usually ignition voltage is higher than the operation voltage [5]. As a high voltage supply Hipotronics (50KV/5mA) model adjustable power supply is used. In the constructed system a fixed operation voltage is used but the current variations are measured. The voltage is raised in order to observe lasing than decreased for a stable beam. Beyond the built in modules in the power supply external ammeter is used to obtain the current measurements

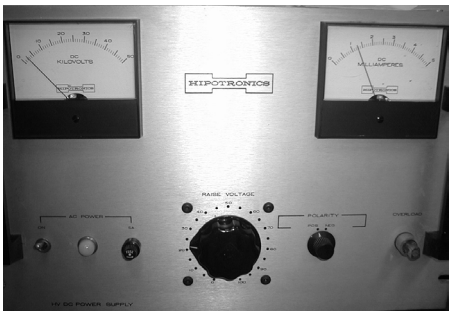

Figure 3.13: HV power supply

3.6. Optical Setup

In order to measure the output power variations caused by the pressure decrease, Coherent Radiation 212 model power meter (Fig 3.13) is used.

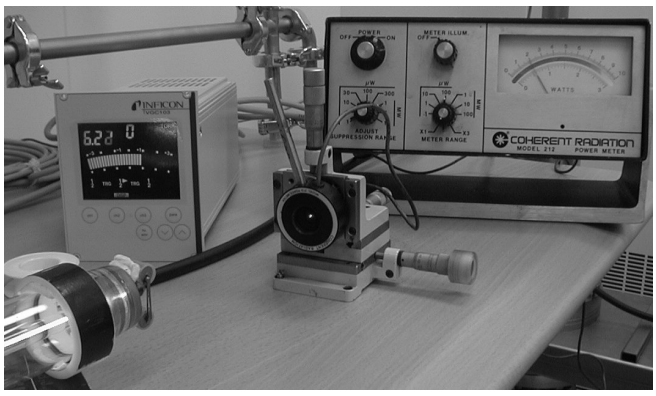

Figure 3.14: Optical power measurement setup

The laser beam spectrum is obtained with Ocean Optics Spectrometer. The output beam is feed to the fiber optic cable.

Spectrometer has a wide band grating and 2048-element linear silicon CCD array detector. Effective range of the spectrometer is 200-1100 nm with a resolution of 1 nm. Given sensitivity is 86 photons/count also, 2.9 x 10^{-17} joule/count, signal-to-noise ratio is 250:1 (at full signal) and dark noise is 2.5-4.0 (RMS).

3.7. Procedure

The experiment can be categorized in four parts; pumping, preparation of gas mixture, filling of the tube with required gas ratio and pressure, and taking data.

The pumping process have been done in two stages; first stage was the pumping with mechanical pump that can reduce the pressure 10^{-2} Torr, then for the second stage the turbo pump was activated. The pumping process takes about 1 hour for the system to decrease to 10^{-5} Torr. For the leak detection, the "helium Leak Check" function of the RGA is used.

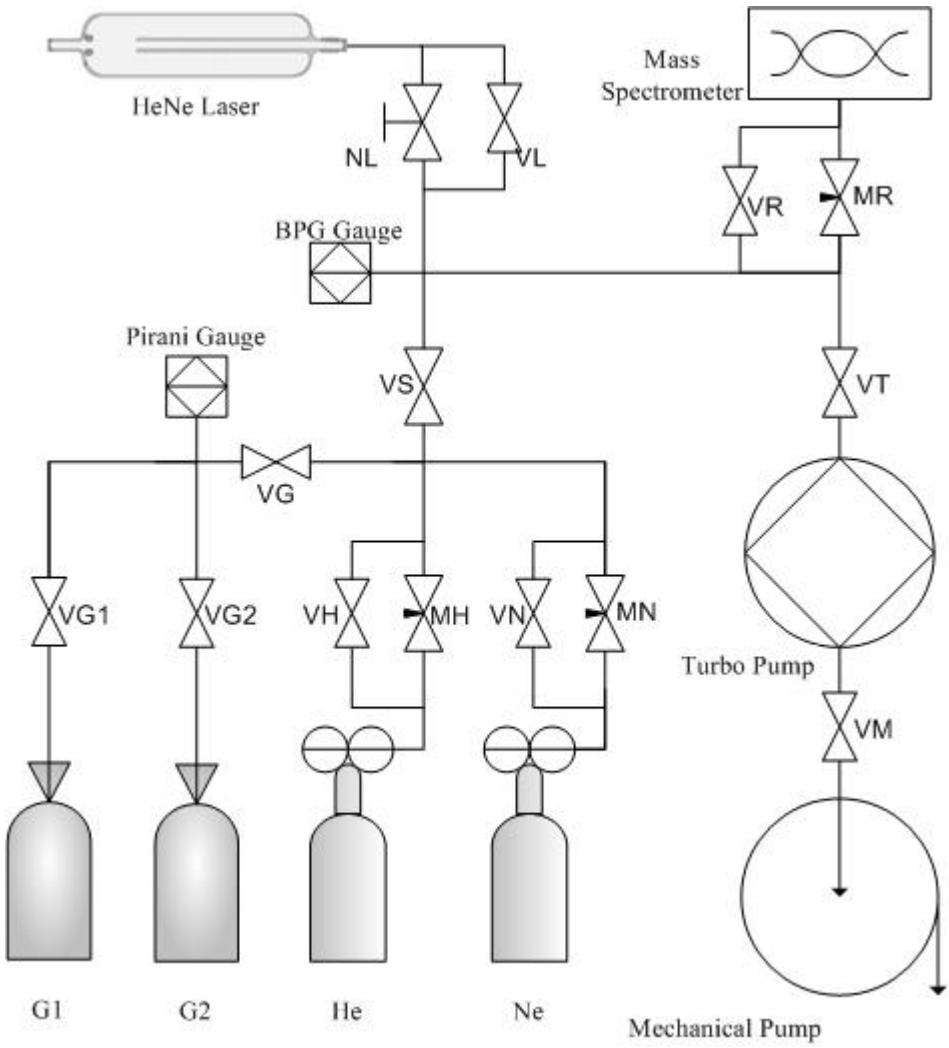

Figure 3.15: Schematic diagram of the vacuum system

The second step was preparation of gas mixture for the laser tube. The Pirani gauge is mainly used to prepare a definite pressure gas mixture. After setting the regulator valve pressure for the gases, the main gas valves [VG]and [MH] are opened , [VT]and [VS] valves are closed and 1st empty gas bottle [G1] is filled with Ne gas by opening the valve [VG1] with pressure indicated in the Table 3,2, after closing the valve [VG1] and [MH], the valves in front of the pump [VT][VS][VG] are opened. The system is pumped again up to 10^{-5} Torr. Then the other gas bottle is filled with Ne gas by opening [VG2] and [MN]. The pressure is adjusted by using the needle metering valves [MH] and [MN]. After closing [VG] the valves of the gas tubes ([VG1] and [VG2]) are opened to mix the gases.

Finally the mixture is filled to the laser tube by opening the valve [VG], [VS] and [NL]. The total pressure of the tube is adjusted by opening the valve [NL] while the system is pumping after the required pressure value is obtained tha valve [N] is closed and the valve [VL] is opened so that some of the gas left out. After waiting for a moment the valve [VN] is closed and the data is taken. This loop continued until the lasing action ends at a high pressure.

Table 3.2: Corrected pressure values for gas mixture preparation (See Sec. 3.3.2)

Ratio	He Pressure (Torr)		Ne Pressure (Torr)	
(He/Ne)	P_{eff}	$P_{ind.}$	P_{eff}	$P_{ind.}$
3.5	3,5	4,38	1	0,71
5	5	6,25	1	0,71
7.5	7,5	9,38	1	0,71
10	10	12,5	1	0,71
13	13	16,25	1	0,71

After filling the required gas ratio the voltage is raised to the breakdown level in order to observe lasing than decreased for a stable beam. The output power of the beam is measured and maximized by adjusting the current.

Before starting the gas mixture preparation process, RGA background data was taken at every time to obtain the impurities and leak data. A graph of the background data is given at Fig.3.16.

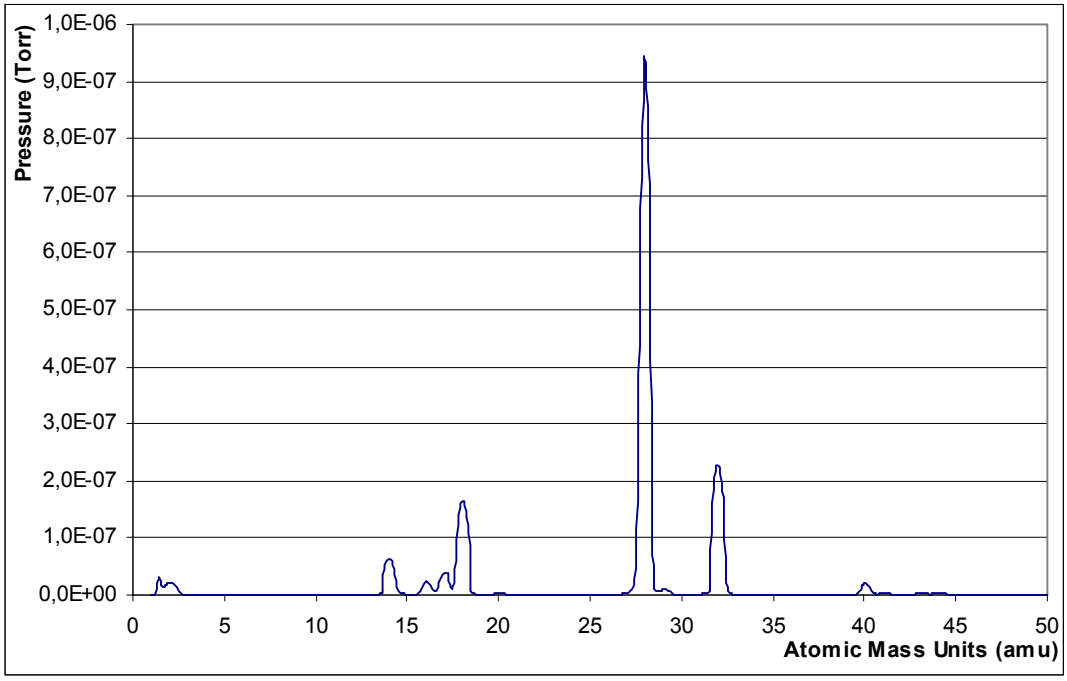

Figure 3.16: Background impurities in the vacuum system.

The corresponding materials for the peak values are given at Table 3.3. It can be understood that the water vapor and Nitrogen peaks are the indicators of a possible leak.

Table 3.3: Atomic mass values for different residual materials.

Material	Atomic Mass
Air	28
CO	28
CO_2	44
H_2	2
He	4
N_2	28
Neon	20
O_2	32
Oil	43
Water	18

CHAPTER 4

RESULTS AND DISCUSSION

4.1. Spectrum Measurements

The spectrum of the laser is measured for all beams at its maximum power. The flux distribution of the obtained spectra was similar except the peak flux. As an example of the recorded spectra the one with a total pressure of 2.18 torr and a mixing ratio of 10/1 is presented in Fig 4.1. It is seen that the relative photon flux density is maximum at 632,8 nm as expected. In plasma state it was possible to see other wavelengths but when it starts lasing the other characteristics wavelengths are disabled. The dielectric coating permits only the required wavelengths.

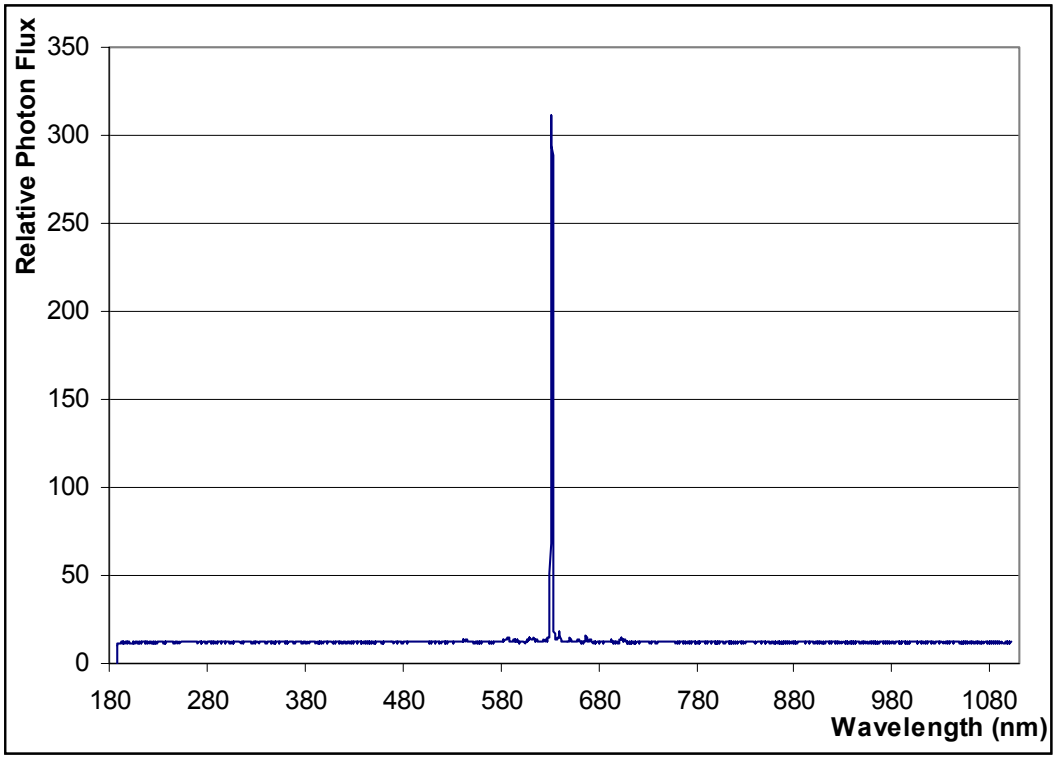

Figure 4.1: Spectrum of HeNe laser at its peak power.

When we look to the graph closer (Fig. 4.2) it is seen that there is a slight peak asymmetry in the spectrum. This may be caused by two reasons; the first one is the wavelength dependent quantum efficiency of the spectrometer, the second one is the spectral contribution of the impurities in the resonator [12]. As stated before the getter is not used in the tube and there were some residual impurities in the system (Fig 3.16).

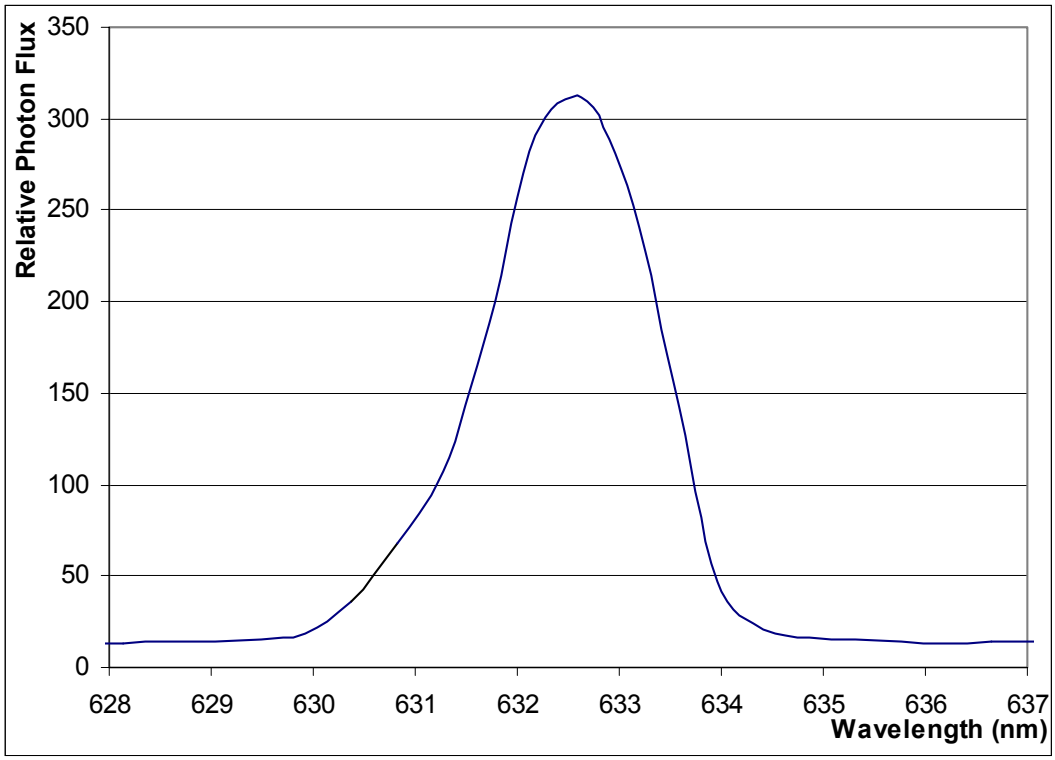

Figure 4.2 : Spectrum analysis of the HeNe laser.

The spectrum analysis show that the FWHM is around 20 Aº, as mentioned before, this value is quite high because of impurity gases in the tube that is mentioned in the last chapter.

4.2. Pressure-Ratio Measurements

Five main clusters of data were measured; with partial pressure ratios of He/Ne; 3.5, 5, 7.5, 10 and 13. The results of these measured values are given in Table 4.1. When the gas ratio varies from 3.5 to 13 it is seen that there is no linear relationship between the ratio and power. And also from the graph (Fig 4.3) the total pressure at maximum power output changes with the gas ratio.

Also the maximum power distribution is not identical in all the pressure rates. At ratio 3.5 the pressure-ratio graph shows a sharper peak than the power at the ratio 13. So in some ratios it is easier to obtain high power values by roughly adjusting the pressure.

Another result is; when the ratio increases, to obtain more power the total pressure should be decreased. It is meaningful that when there is more helium in the cavity, to obtain the population inversion, high pressure is not needed because He 2^1S_0 levels keep the upper 3s neon levels populated. And the 1_S levels of the neon atom can transfer its energy to the helium atom by collision.

Table 4.1: Power output of HeNe laser using the designated pressure values.

Total Pressure (Torr)	He / Ne Gas Partial Pressure Ratio				
	3,5	5,0	7,5	10,0	13,0
5,60	0	0	0	0	0
5,10	0	0	0	0	0
4,60	0	0	0	0	0
4,46	0	0	0	0	0
4,00	0	0	0	0	0
3,75	2,5 µW	0	0	0	0
3,50	8,5 µW	0	0	0	0
3,25	22,0 µW	17,0 µW	4,5 µW	0	0
3,00	25,0 µW	27,0 µW	15,0 µW	0	0
2,75	10,0 µW	30,5 µW	18,0 µW	7,5 µW	1,5 µW
2,55	0,5 µW	31,0 µW	17,5 µW	22,0 µW	5,5 µW
2,43	0	29,5 µW	15,0 µW	28,5 µW	8,5 µW
2,25	0	23,5 µW	11,0 µW	34,5 µW	9,5 µW
2,18	0	20,0 µW	9,5 µW	35,0 µW	10,0 µW
1,74	0	0	0	30,5 µW	9,5 µW
1,55	0	0	0	25,0 µW	8,0 µW
1,25	0	0	0	14,5 µW	2,5 µW
1,12	0	0	0	10,0 µW	0
0,99	0	0	0	6,0 µW	0
0,89	0	0	0	2,0 µW	0
0,88	0	0	0	1,5 µW	0
0,82	0	0	0	0	0
0,75	0	0	0	0	0

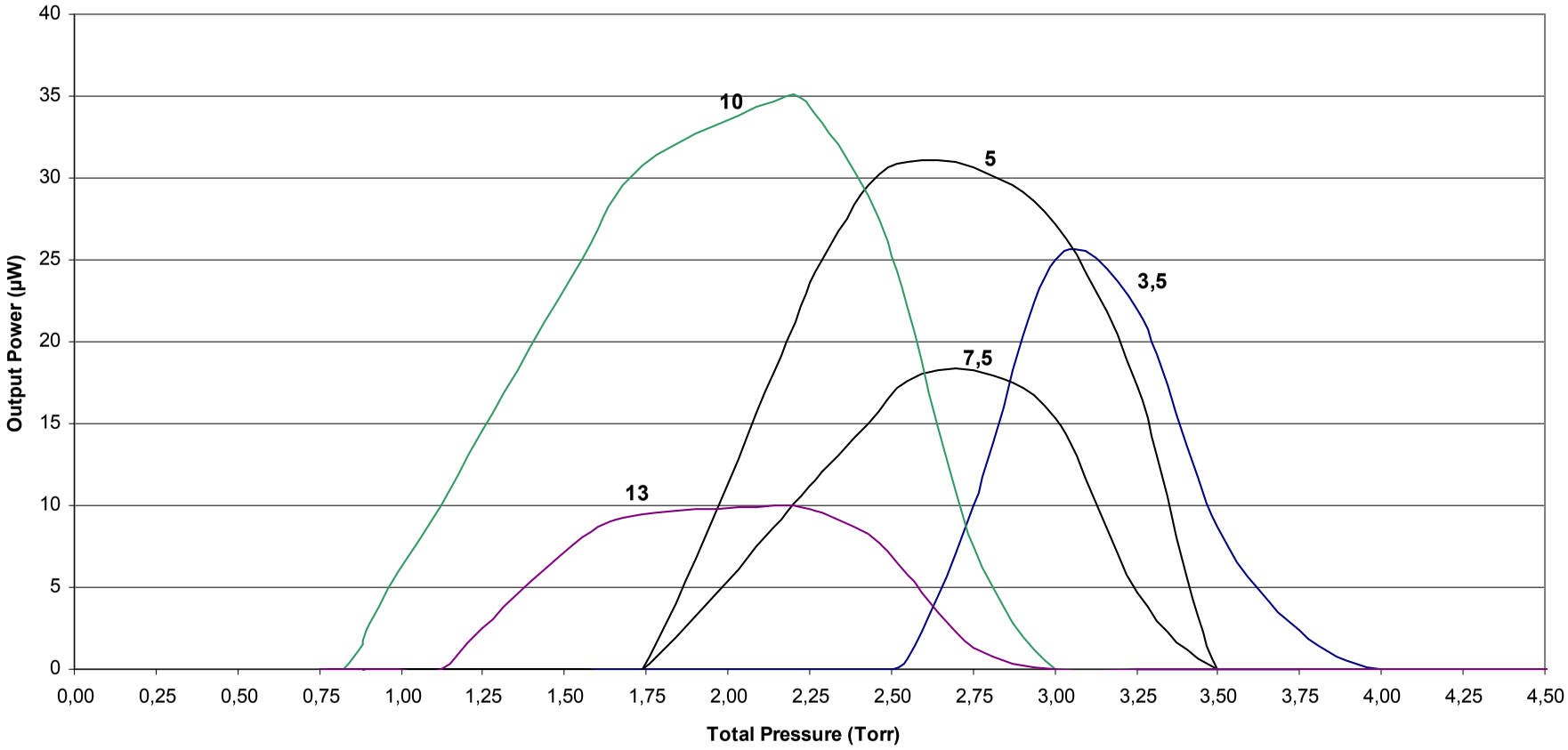

Figure 4.3: Spline smoothed output power for different He/Ne ratios.

4.3. Voltage-Current Measurements

The main electrical parameters that characterize a HeNe laser can be summarized as follows;

- *Discharge voltage :* It is the first break-down voltage that is needed to obtain a glow discharge. After reaching this value the emission occurs in the visible region of the spectrum and the voltage suddenly drops to a more stable operation voltage.

- *Operation voltage interval :* When the glow occurs the voltage can be adjusted to higher values, but after a value the power of the laser output start to decrease. It is important to find the optimum operation voltage of the laser because this working interval is so narrow.

- Operation current interval : This is the value that gives the clues for the properties of the gas discharge.

- Optimum operation current : The maximum power for the laser beam is not occur at the maximum current. To obtain the maximum power from the laser the operation current interval should be scanned to find the best point.

- Series Resistance : To have a stabilized current, load resistance should be calculated and required resistors should be connected to the system. The resistors are used for making the resistance of plasma positive.

- Second break-down Voltage : This voltage is important to obtain the end point for the graph. It is used for calculating the current limitation characteristics.

The electrical gas discharge graph of the plasma system is given at Fig. 4.4. The working interval of the laser is defined as normal glow region shown by B-E.

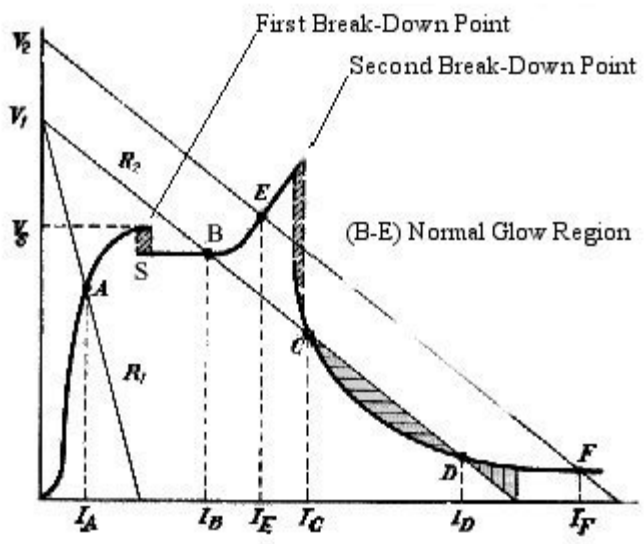

Figure 4.4: Voltage-current behavior of the gas discharge.

The parameters given above are mainly dependent of pressure and the distance between electrodes. Since the described system has built-in cathode and anode structures, the remaining parameter, which is the total pressure of the system, is the key factor for the I-V characteristics. The values of these parameters with different pressures are given below.

Table 4.2: Current and pressure values of gas discharge

Ratio of Partial Pressures (He/Ne)	Total Pressure (Torr)	Laser Power (μW)	Current at Maximum Power (mA)
3,5	3,00	25	1,5
5	2,54	31	3
7,5	2,43	15	3,3
10	2,18	35	3,7
13	2,18	10	3,7

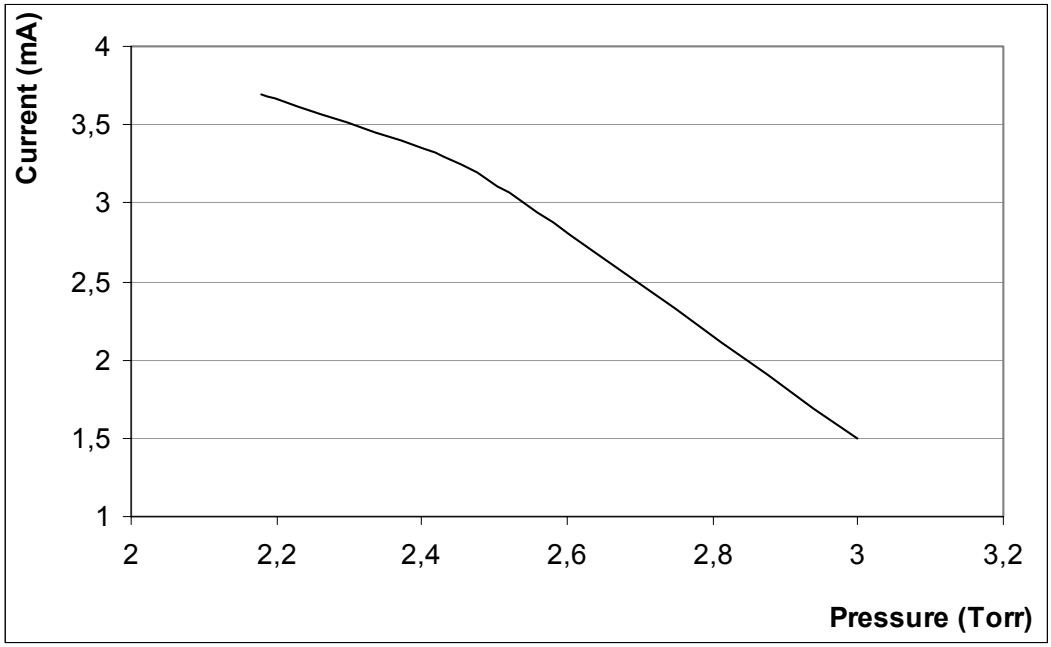

Figure 4.5: Current characteristics of the HeNe gas discharge.

The minimum current occurs at the voltage where first break-down voltage drops to the operation voltage range and it increases with the increasing voltage. When the current is observed at the maximum output power of the laser a graph as shown in Fig 4.5.

During the experiments, for all gas ratios same ignition voltages (first break-down voltage) have been observed. The ignition voltage was 5500 V and the operation voltage (B) has been observed at 2300 V.

The second breakdown voltage cannot be observed because of the high voltage supply. The current protection feature gives an overload error when the current increases above 4 mA.

CHAPTER 5

SUMMARY AND CONCLUSION

The results of this thesis can be summarized as follows;

5.1. Spectrum

It can be seen that the peak wavelength is occurred at 632,8 nm. The intensity (relative photon flux) at this power depends on the factors like the output power of the laser at different pressures and the position of the fiber spectrometer

The spectrum analysis show that the FWHM is around 20 Aº, this value is quite high because of several reasons. The main reason is impurity gases in the tube. This result is obtained by using several different residual gas data and consecutive measurement of laser spectrum. The obtained spectrum graphs are shown below.

Spectroscopic data show that the beam profile is not symmetric with respect to the maximum power wavelength (632.8 nm). The key factor that affects this asymmetry is the impurity in the system. Like a background radiation in an optical system the outgassing of steel walls and leaks in the system caused a background impurity and that caused a broadening and asymmetry in the laser.

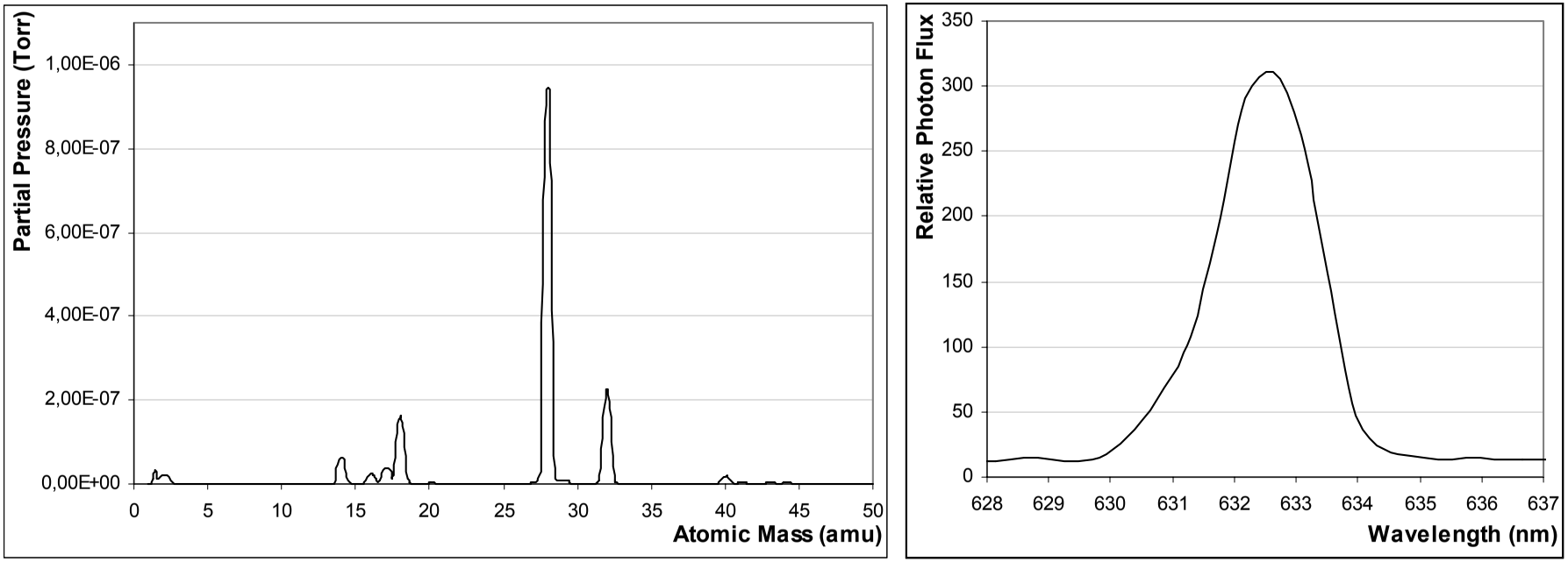

Figure 5.1: Residual Gas Measurement of the tube and the spectrum measurement of the laser (RG1)

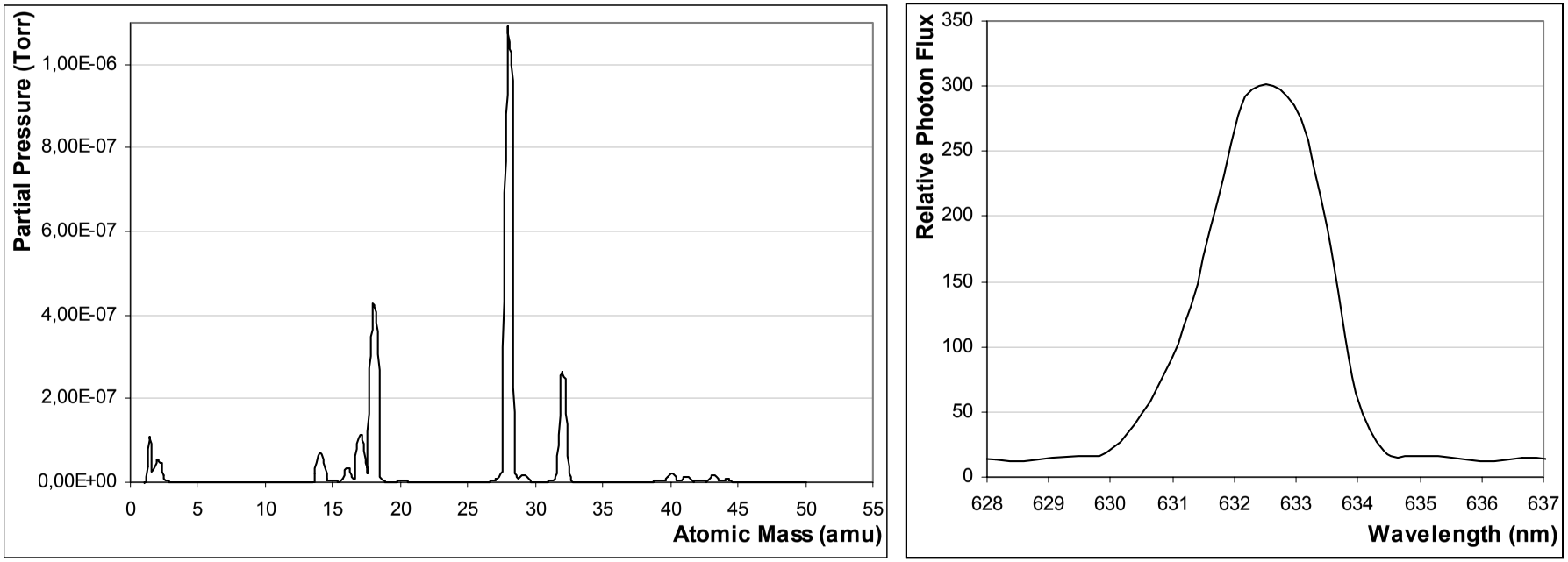

Figure 5.2: Residual Gas Measurement of the tube and the spectrum measurement of the laser (RG2)

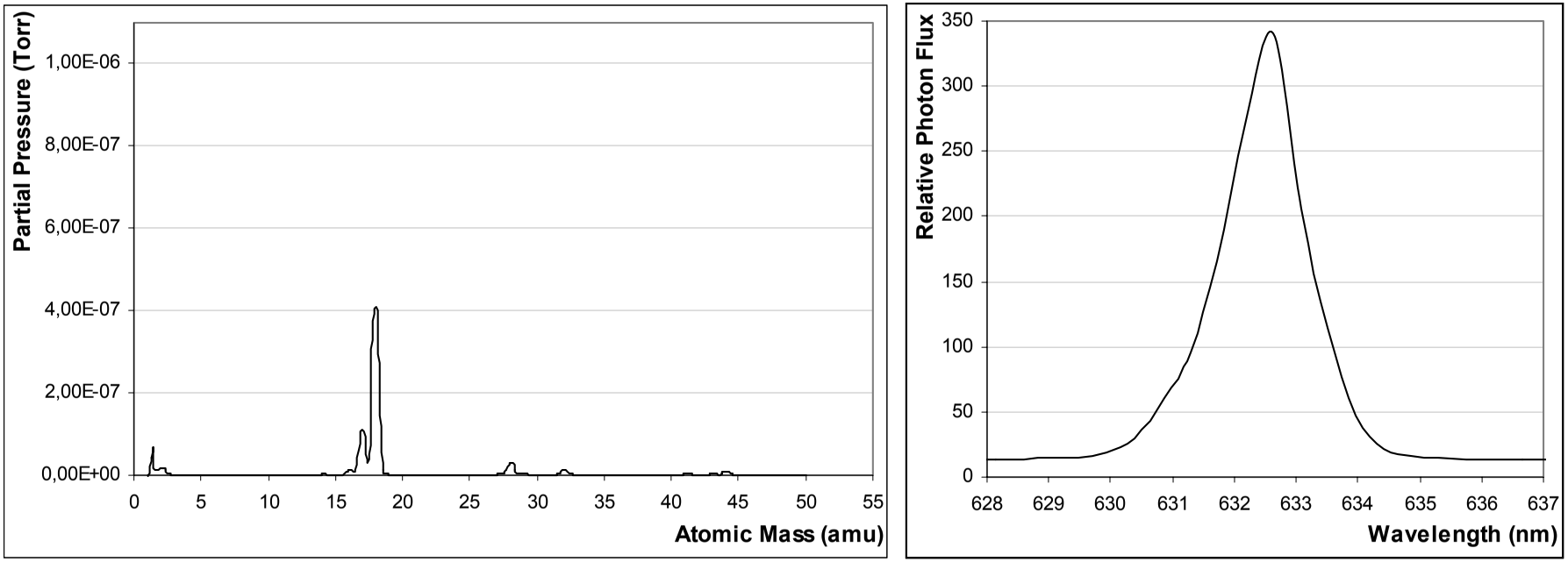

Figure 5.3: Residual Gas Measurement of the tube and the spectrum measurement of the laser (RG3)

The graphs above also show that the leaks in the system (N_2) have a greater effect than the water vapor on the spectrum graph. The broadening and asymmetry of the laser output can be seen more easily in the following graph.

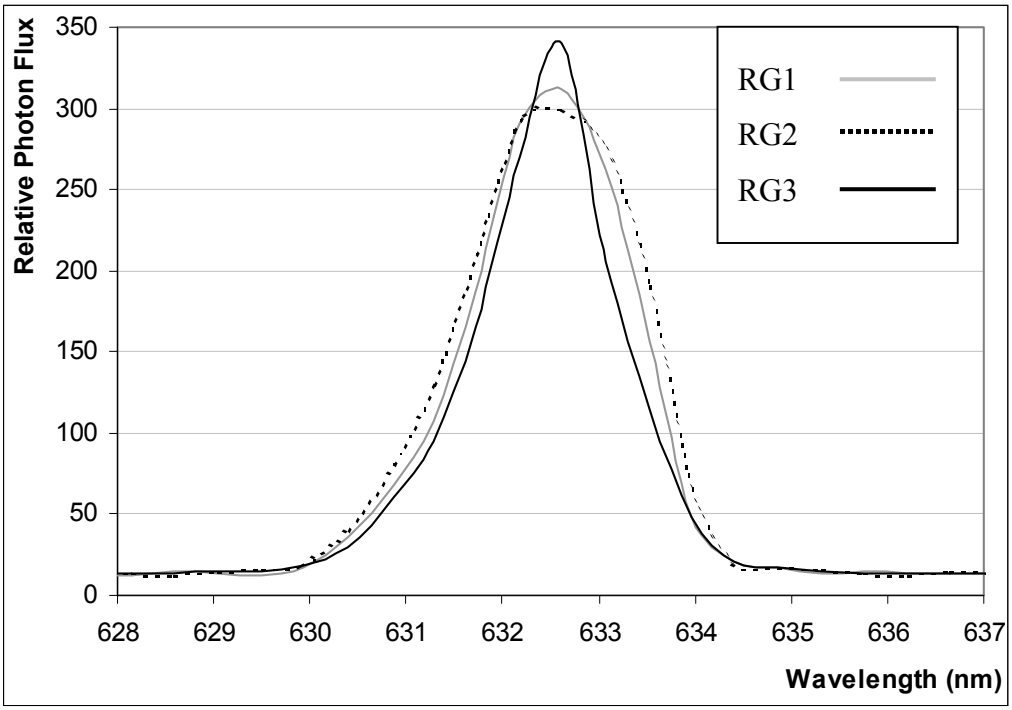

Figure 5.4: Spectrum graph of the laser containing different amount of residual gases

5.2. Total Pressure and Gas Ratio

The capillary diameter and the pressure are the key factors in the HeNe laser system. The total pressure of the HeNe gas is not only affects the excitation voltage-current characteristics but also affects the output power of the HeNe laser.

The ratio of He to Ne is the main parameter for a HeNe laser because of the laser transition mechanism. It can be seen from the Fig.5.5 that changing the gas ratios affect the total pressure of the laser tube which the lasing occurs. But there is not a linear relationship between the two factors.

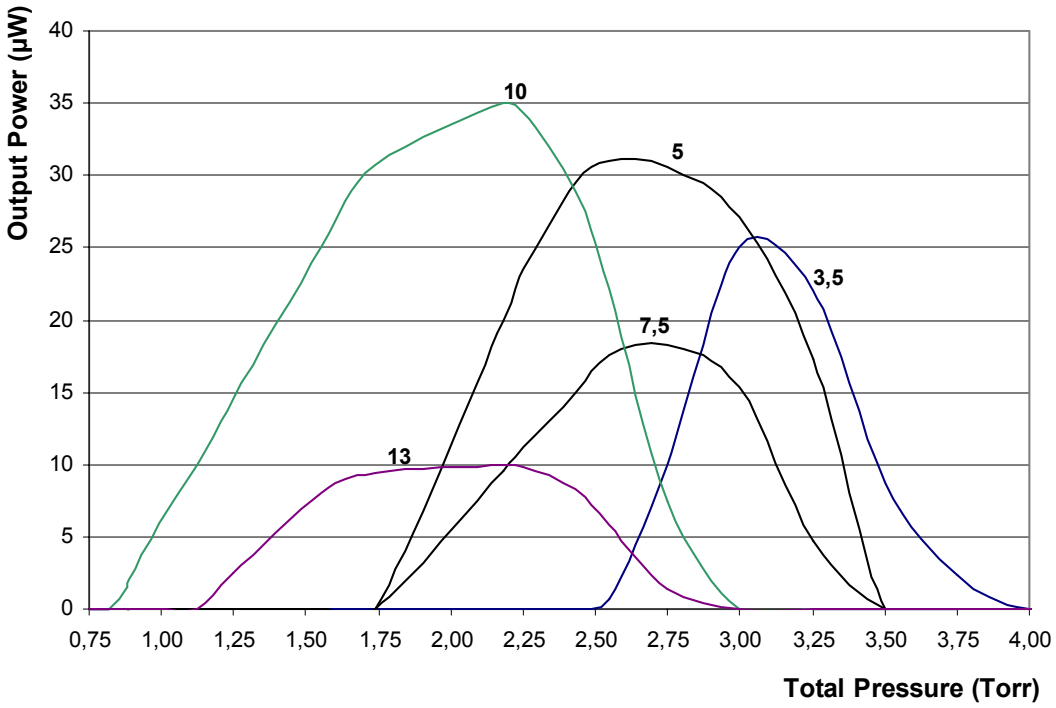

Figure 5.5: Behavior of output power with different gas pressures and ratios.

From the experiments maximum power output is obtained with a pressure of 2,18 Torr and a mixing ratio of He/Ne:10. Another efficient power occurred at 2,55 Torr and ratio of He/Ne:5

5.3. Voltage and Current

When we look at the voltage-current characteristics of different ratios it is obviously seen that the breakdown voltage (5,5 kV) and the operation voltage (2,6 kV) does not depend on the ratios but mainly on total pressures. But since the pressure range is not so wide the change in the voltage can not be distinguished.

The measured current measurements at maximum power outputs gave clues about the laser gain relations. When the pressure of the system increased, the operating current should be decreases to give higher power output (Fig. 5.5).

To limit the operation current, built in series resistors are used; 60KΩ (2x30Ω). So the current-voltage values were found according to optimum resistance.

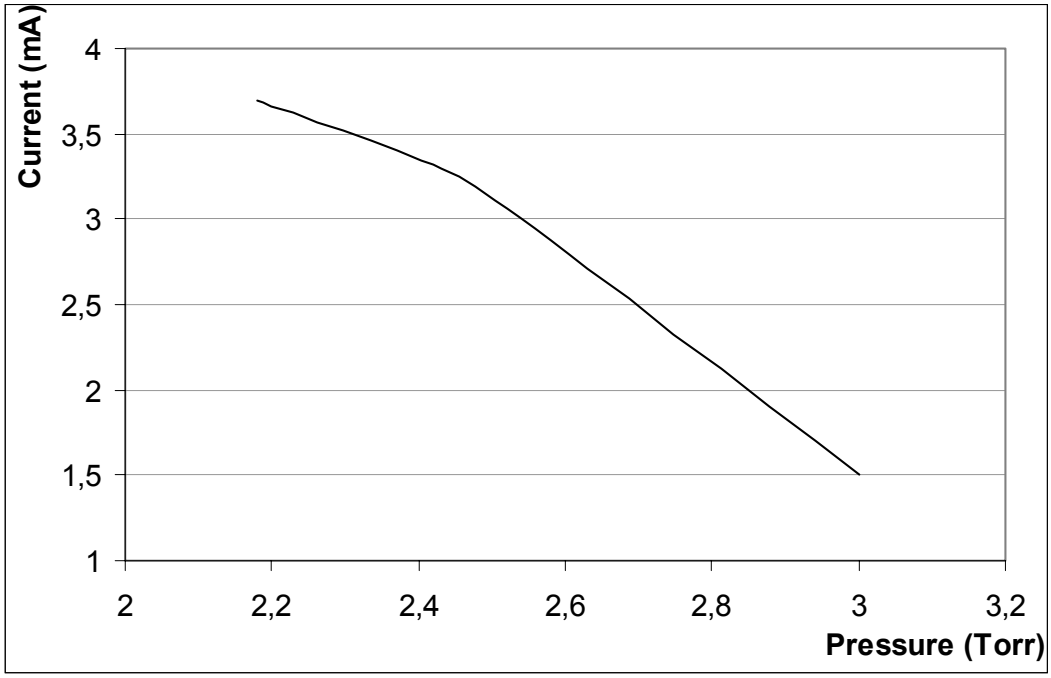

Figure 5.5: Operating current characteristics with different pressure values.

As a result optimum characteristics for a helium-neon laser, such as operation voltage, current, total pressure, partial pressure ratios, are obtained. The values that are found in the experiments are specific values for the laser tube used. But these data form the basis to build a stable HeNe laser.

REFERENCES

[1] A. Javan, W.R. Bennett Jr., D. R. Herriot, “Population Inversion and continuous optical maser oscillation in a gas discharge containing a He-Ne mixture”, Physical Review Letters, Vol. 6, p.106,1961

[2] John Hawkes, Ian Latimer, “Lasers: Theory and Practice”, Prentice Hall, 1994, p.325

[3] Inficon Pirani Standard Gauge, Operating Manual, 2001, p2

[4] Inficon Bayard-Alpert Pirani Gauge, Instruction Sheet, 2004, p1

[5] Werner Reif, “Current-voltage characteristics of glow discharges in narrow Capillaries”, J.Phys.D:Appl.Phys., Vol.12, 1979, p.1721

[6] J-M Chartier et C Garreau, “Sauvetage de tubes de lasers à He-Ne usages", J.Phys.E:Sci. Instrum., Vol.12, 1979, p.913

[7] RGA 100 Residual Gas Analyser, Operating Manual and Programming Reference, R1.5, 2004, p.2-8

[8] Pirani Standard Gauge Product Guide, http://www.inficon.com/

[9] P.W. Smith, “The output power of a 6328 Å He-Ne gas laser”, IEEE J. Quantum electronics, Vol.QE-2, 1966, p.62

[10] W. Espe, M. Knoll, and M. P. Wilder, “Getter Materials for Electron Tubes”, Electronics Magazine, 1950, p.85

[11] W. P. Kolb, “Five-Year Operation of a He-Ne Laser”, IEEE J. Quantum electronics, Vol.QE-2, 1975, p.374

[12] Charles C. Allgood, “Impact and behavior of trace contaminants in high purity plasma process gases”, Solid State Technology, Sept. 1999, p. 63

[13] A.L. Bloom, “Gas Lasers”, John Wiley & Sons, 1968, p.51

[14] “HeNe-Laser Experiment Manual”, MEOS, 1993, p.5

[15] A.D. White, J.D. Ridgen, “Continuous gas maser operation in the visible spectrum”, Poc. IRE., Vol. 50, 1962, p.1967

APPENDIX

Table A.1: Spectrum vs Intensity data of HeNe Laser

Wavelength	Relative Photon Flux		
(nm)	RG1	RG2	RG3
627,69	12	13,2	15
628,14	12	13	14
628,59	15	13,7	12
629,04	13	14,3	15
629,49	12	14,8	16
629,93	17	18,2	19
630,38	36,1	30	40
630,86	68	60	80
631,28	107,6	95	130
631,73	187,7	165	210
632,17	291,1	270	292
632,62	311,2	340	300
633,07	263,1	205,3	275
633,52	156,6	115	190
633,97	47,5	47,5	65
634,41	21,2	21,2	20
634,86	16,7	16,7	16,7
635,31	14	15	16
635,76	15	14	13
636,2	13	13,4	12
636,65	13	14	15
637,1	14	13,8	13